Desulfurization from Liquid Fuels by Decomposition of Aromatic Sulfur Compounds under Ultraviolet Irradiation

篠﨑, 貴旭

Desulfurization from Liquid Fuels by Decomposition of Aromatic Sulfur Compounds under Ultraviolet Irradiation

Graduate School of Science

Kyushu University

Taka-Aki SHINOZAKI

December 2022

Contents

Abstract

In the production of liquid fuels from petroleum, hydrodesulfurization methods that reduce the amount of sulfur contained as impurities to 10 mg(S)/L (weight/volume concentration of sulfur, which is equivalent to 0.31 mmol/L in molar concentration) or less are widely used. In particular, the desulfurization of aromatic sulfur compounds, such as benzothiophene derivatives (BTs) and dibenzothiophenes derivatives (DBTs), requires catalytic processes at high temperature (200–400 ℃) and high pressure (5–80 atm). In recent years, to reduce both the burden on the global environment and costs, desulfurization methods with room temperature and atmospheric pressure operating parameters must be developed.

In this study, the author develops a method for desulfurizing aromatic sulfur compounds, such as BTs and DBTs, at room temperature and atmospheric pressure without the use of additives and catalysts. When BTs and DBTs are irradiated with 8 W ultraviolet (UV) light (254 nm,), the decomposition of both BTs and DBTs reaches 100 % in approximately 8 and 16 h, respectively. In addition, a yellow precipitate is deposited as they decompose. Analysis of the precipitate by X-ray fluorescence, high-performance liquid chromatography, and atmospheric pressure solid analysis probe-mass spectrometry reveals that the precipitate consists of allotropes of sulfur (S_n). In addition, the decomposition products of the hydrocarbon portion of BTs and DBTs after sulfur removal were identified, and benzene was detected, suggesting that benzene was formed as one of the degradation products. These results suggest that when BTs and DBTs are irradiated with UV light, the sulfur content is converted to allotropes of sulfur (S_n) and the hydrocarbon portion decomposes via benzene. Furthermore, the reaction kinetics of the decomposition reaction by UV light irradiation are investigated and the reaction is found to be of pseudo-first-order. To elucidate the reaction mechanism, a theoretical investigation is performed using density functional theory calculation.

Chapter 1

1. General Introduction

The petroleum of animal and plant origins contains a few percent of organic and inorganic sulfur compounds[1]. Crude oil is separated into refinery fuel (< 35 °C), gasoline (35–180 °C), kerosene (150–280 °C) and diesel (180–350 °C) by distillation. Generally, fuels desulfurized to 10 mg(S)/L (weight/volume concentration of sulfur, which is equivalent to 0.31 mmol/L in molar concentration) or less are supplied in Japan, the United States, Europe, and other developed regions; however, in regions such as South America and South Africa, setting up large-scale desulfurization equipment is challenging. Thus, adequate desulfurization is not possible, and fuels with high concentrations (10 mg(S)/L ≤) of sulfur are being supplied in these areas (**Figure 1-1)**[2].

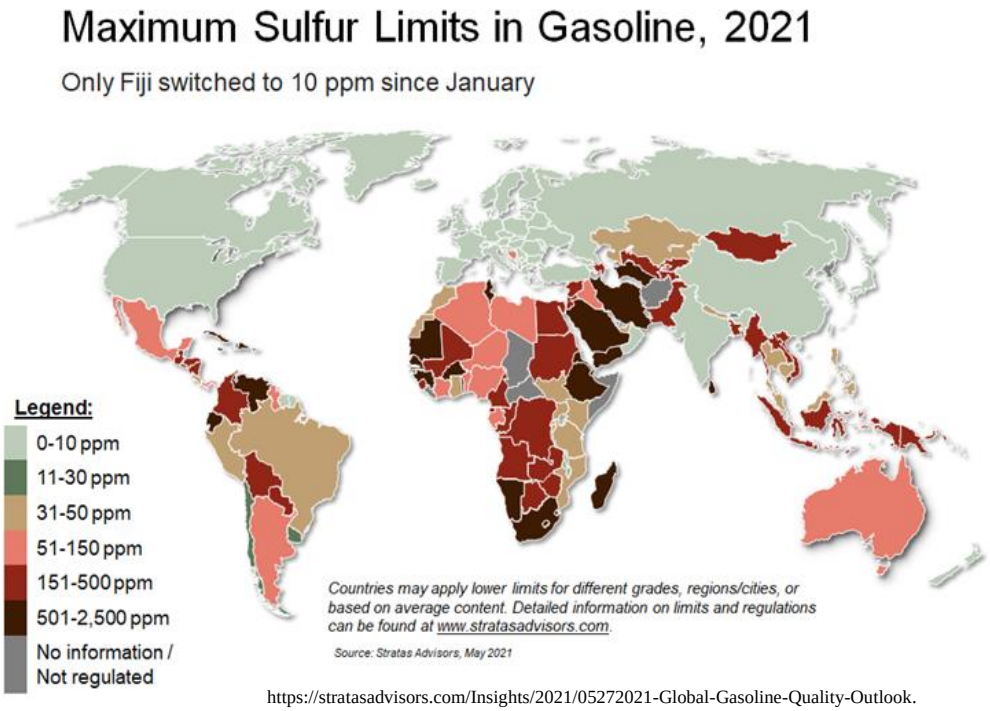

https://stratasadvisors.com/Insights/2021/05272021-Global-Gasoline-Quality-Outlook.

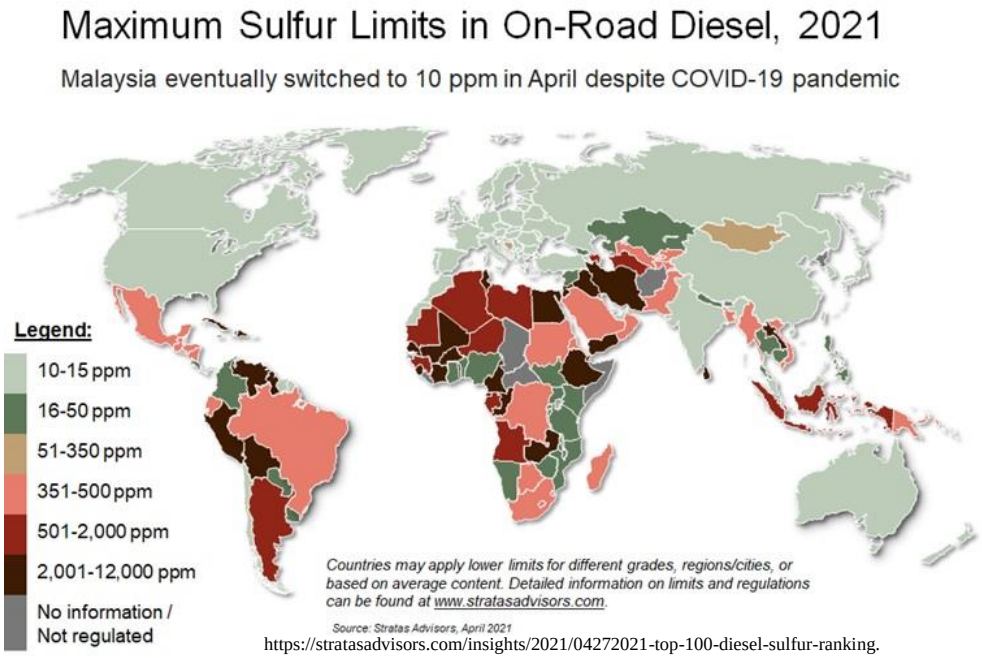

https://stratasadvisors.com/insights/2021/04272021-top-100-diesel-sulfur-ranking.

Figure 1-1: Regulated sulfur limits for petroleum-based fuels[3-4].

Burning fuels with high concentrations of sulfur produces sulfur oxides, which cause acid rain and air pollution. Further, part of the burned sulfur turns into sulfates, which are suspended particulate matter that can affect the human body[5]. Additionally, sulfates react in the atmosphere and form particulate matter ($PM_{2.5}$ and PM_{10}), a carcinogenic pollutant[6-7]. In Japan, sulfurous acid gas generated by the combustion of sulfur contained in petroleum had caused a number of pollution-related illnesses, such as Yokkaichi asthma, first identified in the late 1960s[8]. This led to the enactment of the Air Pollution Control act and the regulation of maximum levels of sulfur in fuels.

Petroleum contains various sulfur compounds, including thiols, sulfides, and cyclic and aromatic sulfur compounds. Some typical aromatic sulfur compounds and their structures are summarized in **Figure 1-2**[9]. These compounds has been decomposed by hydrodesulfurization under high temperature (200–400 °C) and pressure (5–80 atm) in the presence of a highly active catalyst[10-12].

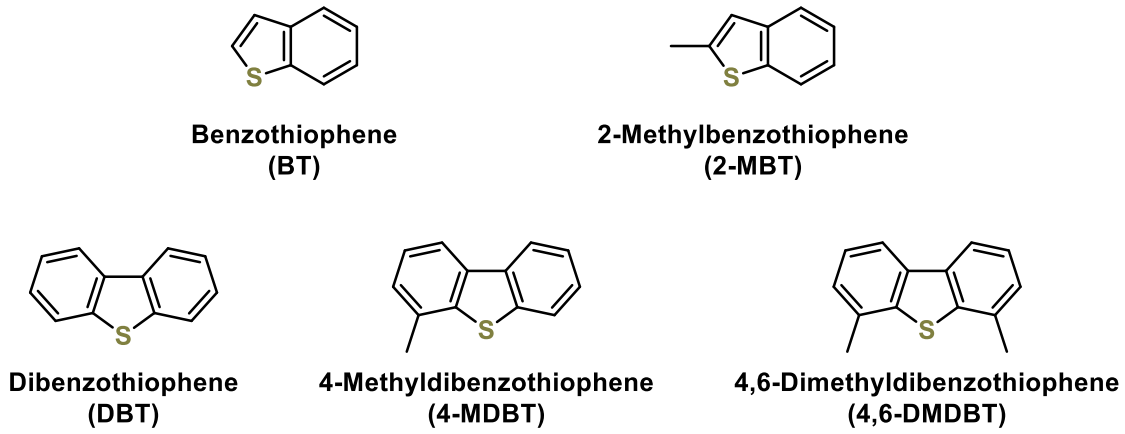

Figure 1-2: Typical aromatic sulfur compounds found in petroleum.

However, aromatic sulfur compounds difficult to desulfurize because they have large steric hindrance, high stability, and low ability to coordinate with catalysts. The difficulty in desulfurization depends predominantly on the substituents around the sulfur atoms in dibenzothiophenes derivatives (DBTs). Alkyl DBT derivatives, such as 4,6-DMDBT, are more difficult to desulfurize compared with DBT; the order according to the degree of difficulty is DBT < 4-MDBT < 4,6-DMDBT[13]. Therefore, an efficient ultra-deep desulfurization method (<10 mg(S)/L) for these compounds must be developed.

In recent years, oxidative desulfurization (ODS)[14-16], extractive desulfurization (EDS)[17-20], and biological desulfurization (BDS)[21-23] have been developed as alternative methods to hydrodesulfurization. In the ODS process, DBT is oxidized and removed as dibenzothiophene-5,5-dioxide ($DBTO_2$) using an oxidant under low temperature and atmospheric pressure conditions. (**Scheme 1-1**).

(a) Reaction using oxygen and transition metal catalyst (Nomura et al, 2003)

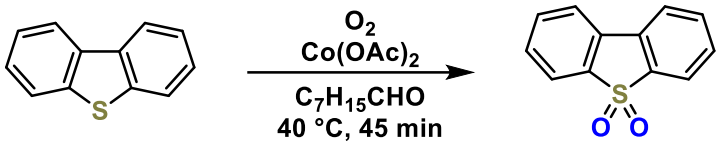

(b) Oxidation reaction using hydrogen peroxide and acetic acid (Nazem et al, 2009)

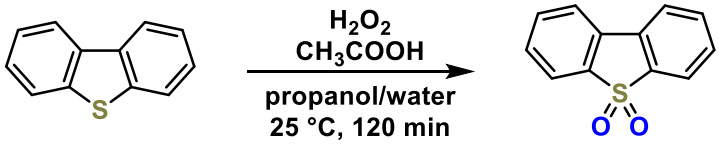

Scheme 1-1: Oxidation of DBT with transition metals and oxidizing agent.

Desulfurization using ionic liquids (ILs) is an extraction desulfurization method. ILs have very low vapor pressures; further, they are thermally and chemically stable, nonflammable, noncorrosive, and versatile. Thus, ILs selectively removes sulfur compounds with the aid of the interactions (*e.g.*, π–π interaction, electrostatic force, hydrogen bond, etc.) between ionic liquids and aromatic sulfur compounds (**Scheme 1-2**).

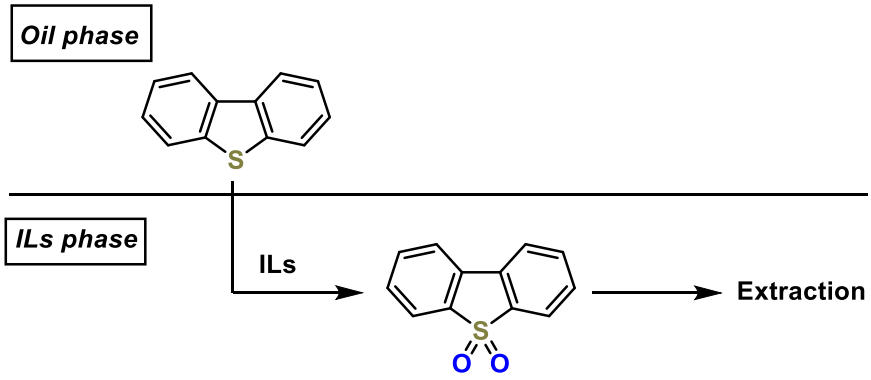

Scheme 1-2: Schematic of simultaneous two-phase oxidation and extraction desulfurization.

BDS is an enzyme-based method (using DBT monooxygenase: DszA, DszB, DszC, and DszD) that has been proposed as a cost-effective and environmentally safe sulfur removal process (**Scheme 1-3**).

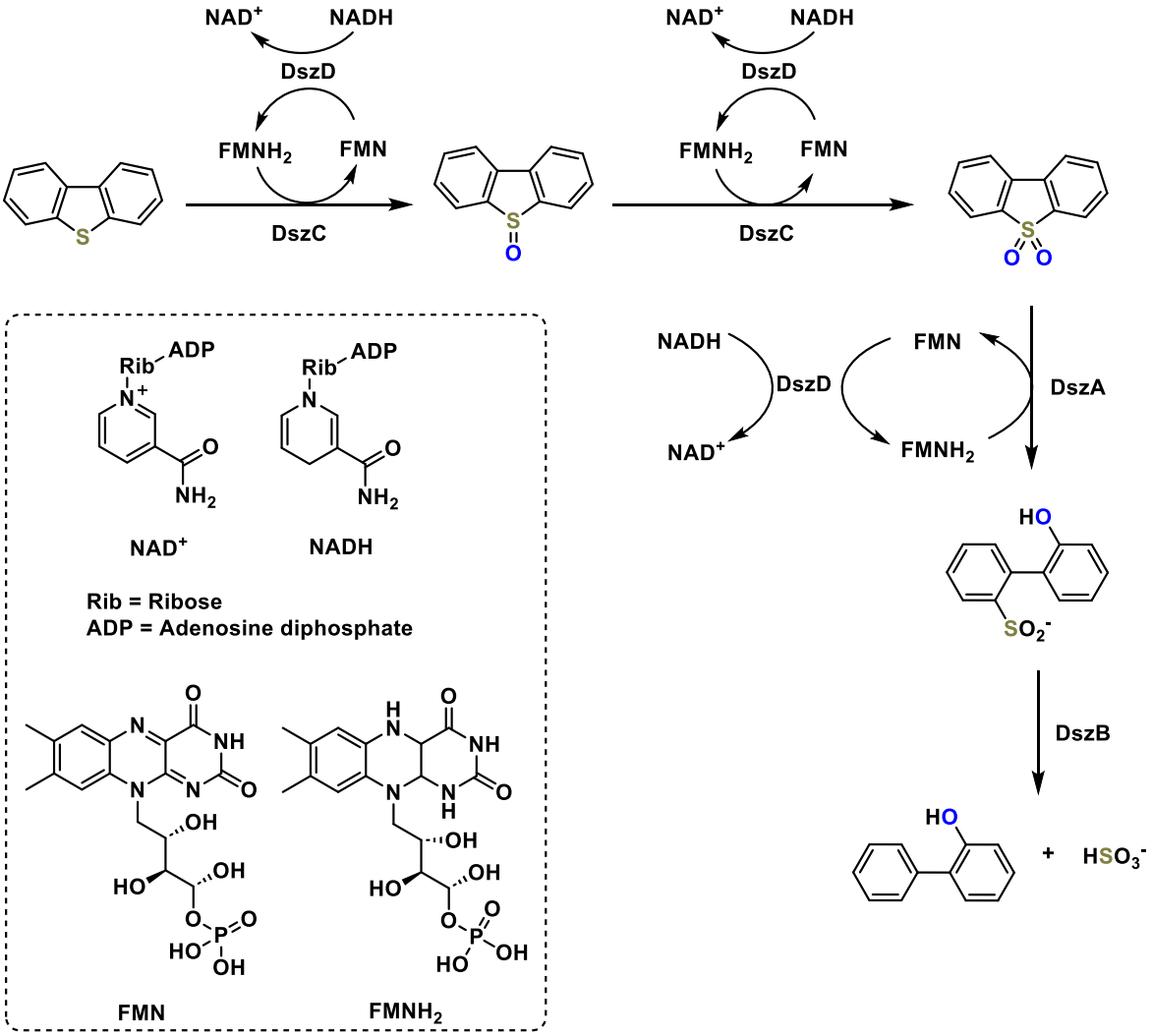

Scheme 1-3: Degradation mechanism of DBT using enzyme.

However, ODS requires a strong oxidant with sacrificial reagents (H_2O_2, CH_3COOH and R-CHO). EDS using ILs is insoluble in fuel and requires an extraction operation. In addition, BDS has the disadvantage in that the desulfurization is time consuming. In all three cases, numerous issues remain, which need to be solved to allow their practical application.

In Japan, sulfur was mined in sulfur mines from the end of the 19th century until 1960, and was widely used as a raw material for explosives, chemical fertilizers, and synthetic rubber. However, numerous sulfur mines were closed when Krause discovered a method for sulfur production using hydrogen sulfide, a byproduct of petroleum hydrodesulfurization. The Krause process burns one-third of the generated hydrogen sulfide to sulfur dioxide, which is subsequently reduced with the remaining hydrogen sulfide to produce solid sulfur[24].

$$H_2S + \frac{3}{2}O_2 \rightarrow SO_2 + H_2O$$

$$2H_2S + SO_2 \rightarrow \frac{3}{8}S_8 + 2H_2O$$

In addition, sulfur oxide, carbonyl sulfide and carbon disulfide remain in the tail gas treated in the Krause process but are reduced to hydrogen sulfide in the Shell Claus Of gas Treater (SCOT) process and reused in the Krause process[24]. The combination of the Krause and SCOT methods enables the recovery of sulfur from hydrogen sulfide to be >99 %; however, it requires a multi-step reaction with catalysts under conditions of high temperature, high pressure, which typically requires a large facility.

$$SO_2 + 3H_2 \rightarrow H_2S + 2H_2O$$

$$SO_3 + 4H_2 \rightarrow H_2S + 3H_2O$$

$$COS + 4H_2 \rightarrow H_2S + CH_4 + H_2O$$

$$CS_2 + 4H_2 \rightarrow 2H_2S + CH_4$$

Heying et al reported a theoretical study on the photodecomposition of thiophene. Irradiating thiophene with light leads to its oxidation into thiophene oxide (TO), thus producing furan. Subsequently, homolytic cleavage of the S–C bond, a 6π electrocyclic reaction, thiirane formation, and elimination of the S atom occur (**Scheme 1-4**)[25].

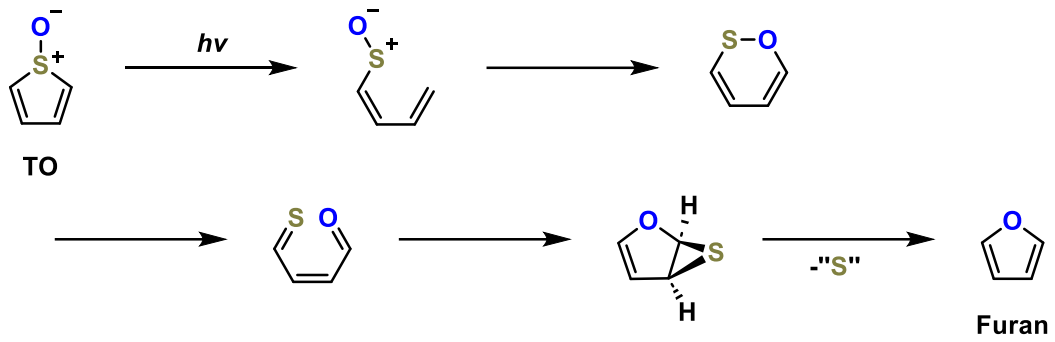

Scheme 1-4: Furan formation from TO using theoretical calculations by Heying group[25].

Also, Korang et al. theoretically predicted that the irradiation of dibenzothiophene-5-oxide derivatives (DBTOs) causes the reaction to proceed along a similar pathway, shown in **Scheme 1-5**[26]. However, the elimination of S atoms and verification of the decomposition products after light irradiation have not yet been confirmed experimentally.

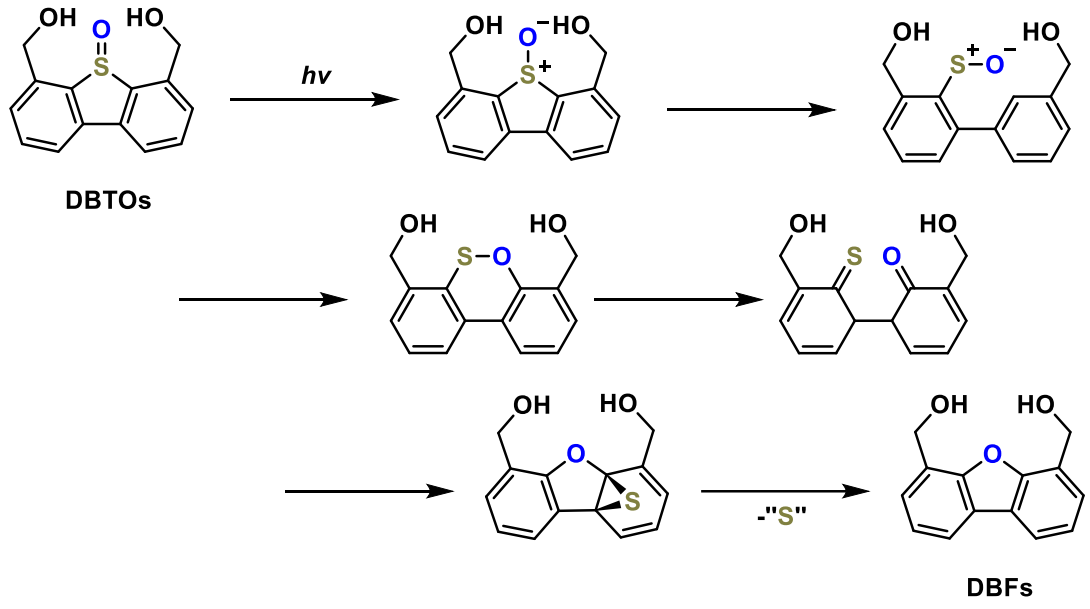

Scheme 1-5: Conversion from DBTOs to dibenzofuran derivatives (DBFs) using light irradiation, as proposed by the Korang group[26].

Based on these reports, the author thought that if the author could separate only sulfur in fuels using photo-oxidation of sulfur compounds, the author could construct a low-cost desulfurization process that is more energy-efficient and easier to operate the reaction than previous reports. Specifically, the author developed a reaction in which aromatic sulfur compounds are oxidized by ultraviolet (UV) irradiation (λ=254 nm) by 8 W lamp to remove sulfur contained in BTs and DBTs as sulfur allotropes (S_n), and the remaining hydrocarbons are recycled as fuel (**Scheme 1-6)**. In addition, photodegradation kinetics were investigated and the degradation mechanism was examined using density functional theory (DFT) calculations.

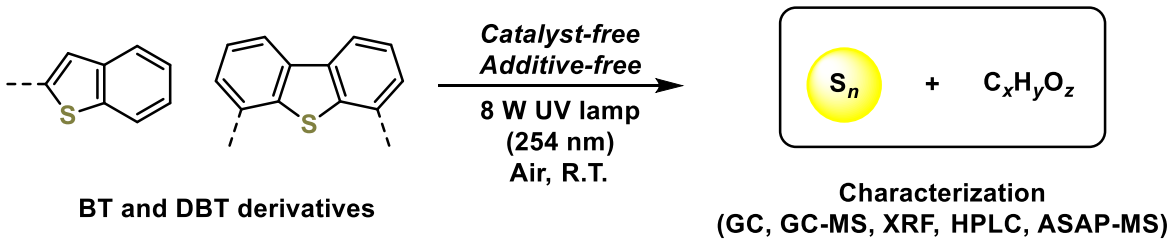

Scheme 1-6: Photodecomposition reactions of selected aromatic sulfur compounds.

Reference

1. Hsu, C.S., Robinson, P.R. 2006. Practical Advances in Petroleum Processing. Springer, New York. Volumes 1. Chapter 2.
2. Yashnik, S.A., Kerzhentsev, M.A., Salnikov, A.V., Ismagilov, Z.R., Bourane, A., Koseoglu, O.R. *Kinet. Catal.* **2015**, *56*, 466-475.
3. https://stratasadvisors.com/Insights/2021/05272021-Global-Gasoline-Quality-Outlook
4. https://stratasadvisors.com/Insights/2021/04272021-Top-100-Diesel-Sulfur-Ranking
5. Rall, D.P. *Environ. Health Perspect.* **1974**, *8*, 97-121.
6. https://www.epa.gov/pm-pollution/particulate-matter-pm-basics#PM/2018.
7. Zhang, R., Wang, G., Guo, S., Zamora, N.L., Ying, Q., Lin, Y., Wang, W., Hu, M., Wang, Y. *Chem. Rev.* **2015**, *115*, 3803-3855.
8. Katsumi, Y., Hidehiko, O., Masayuki, I. *Arch Environ Health.* **1966,** *13*, 763.
9. Andari, M.K., Behbehani, H., Qabazard, H. *Fuel Science and Technology International.* **1996**, *14(7)*, 897-908.
10. Desikan, P., Amberg, C.H. *Can. J. Chem.* **1964**, *42*. 843-850.
11. Houalla, M., Nag, N.K., Sapre, A.V., Broderick, D.H., Gates, B.C. *AIChE J.* **1978**, *24(6)*, 1015-1021.
12. Kwart, H., Schuit, G.C.A., Gates, B.C. *J. Catal.* **1980**, *61*, 128-134.
13. Kilanowski, D.R., Teeuwen, H., DeBeer, V.H.J., Gates, B.C., Schuit, G.C.A., Kwart, H. *J. Catal.* **1978**, *55*, 129-137.
14. Murata, S., Murata, K., Kidena K., Nomura, M. *Energy Fuels,* **2004**, *18*, 116-121.
15. Dehkordi, A.M., Sobati, M.A., Nazem, M.A. *Chin. J. Chem. Eng.* **2009**, *17(5)*, 869-874.
16. Houda, S., Lancelot, C., Blanchard, P., Poinel, L., Lamonier, C. *Catalysts.* **2018**, *8*, 344-369.
17. Eßer, J., Wasserscheid, P., Jess, A. *Green Chem.* **2004**, *6*, 316-322.

18. Yu, F., Liu, C., Yuan, B., Xie, P., Xie, C., Yu, S. *Fuel*. **2016**, *177*, 39-45.

19. Raj, J.J., Magaret, S., Pranesh, M., Lethesh, K.C., Devi, W.C., Mutalib, M.I.A. *J. Clean. Prod.* **2019**, *213*, 989-998.

20. Xu, Y., Liu, L., Bu, Y., Chen, M., Wang, L. *J. Clean. Prod.* **2021**, *284*, 124788-124801.

21. Gray, K.A., Mrachko, G.T., Squires, C.H. *Curr. Opin. Microbiol.* **2003**, *6*, 229-235.

22. Nassar, H.N., Amr, S.S.A., El-Gendy, N.S. *Environ. Sci. Pollut. Res.* **2020**, *28*, 8102-8116.

23. Sousa, J.P.M., Ferreira, P., Neves, R.P.P., Ramos, M.J., Fernandes, P.A. *Green Chem.* **2020**, *22*, 7604-7621.

24. Hsu, C.S., Robinson, P.R. 2017. Springer Handbook of Petroleum Technology. Springer, New York. Chapter 20.

25. Heying, M.J., Nag, M., Jenks, W.S. *J. Phys. Org. Chem.* **2008**, *21*, 915–924.

26. Korang, J., Grither, W.R., McCulla, R.D. *J. Am. Chem. Soc*. **2010**, *132*, 4466–4476.

Chapter 2

2 Results and discussion

2-1 Optimization of reaction conditions

As an initial study, BTs and DBTs were dissolved in hexane, a component of petroleum, and irradiated with 8W UV light (254 nm) for 24 h. Analysis of the solution after UV light irradiation using gas chromatography-flame ionization detector (GC-FID) revealed that the BTs and DBTs were no longer present. Therefore, the light intensity was determined to be sufficient. However, several peaks at the mg/L concentration levels were observed, and the chromatograph was too complex to determine all the degradation products derived from the BTs and DBTs (**Figure 2-1**).

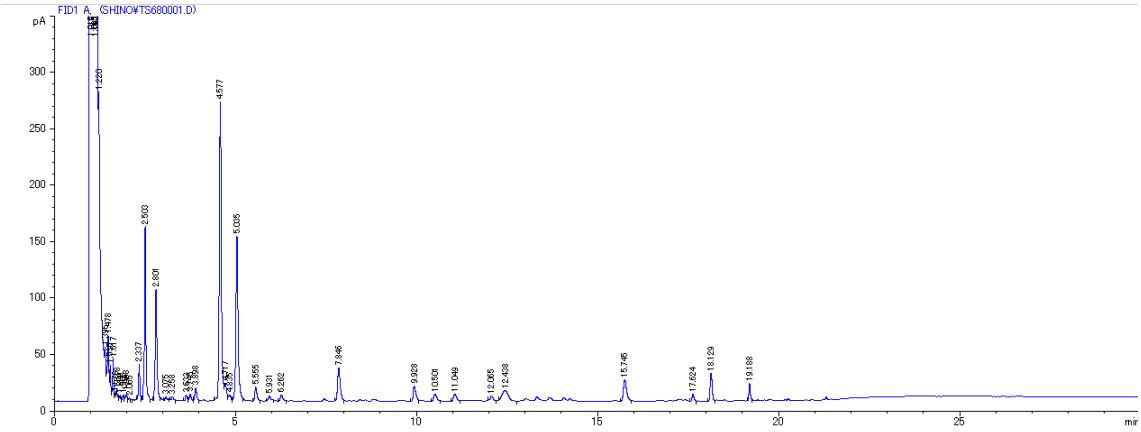

Figure 2-1: GC-FID chromatogram after 8 W UV (254 nm) irradiation (24 h) in hexane.

According to gas chromatography-mass spectrometry (GC-MS) analysis, most of these peaks were derivatives of the hexane solvent, either oxidized or dimerized. Although the oxidation of saturated hydrocarbons in meaningful yields via UV irradiation has not been reported thus far, they are assumed to be formed by radical reactions in the presence of oxygen in air. To reduce the number of these compounds produced by solvent oxidation, cyclohexane was chosen because of its high symmetry. Consequently, the solvent-derived byproducts could be reduced to three compounds, namely cyclohexanol, cyclohexanone, and dicyclohexyl ether (**Figure 2-2**). Based

on these results, cyclohexane was chosen as the solvent in this study.

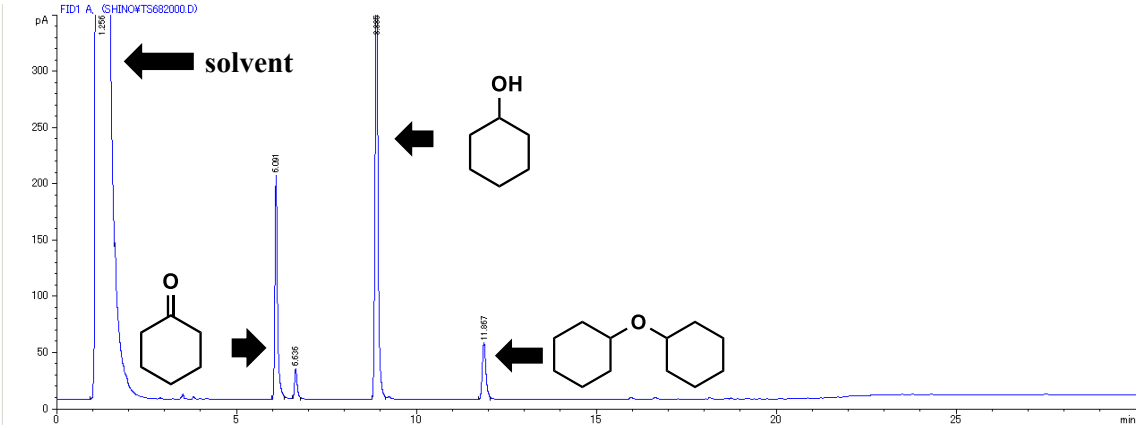

Figure 2-2: GC-FID chromatogram after 8W UV (254 nm) irradiation (24 h) in cyclohexane.

2-2 UV spectra and desulfurization of BTs and DBTs by UV irradiation

The UV absorption spectra of solutions of BTs and DBTs in cyclohexane revealed strong absorption in the UV region of 230–270 nm with similar shapes for the spectra (**Figure 2-3(a)**). Based on the absorption properties, BT, 2-MBT, DBT, 4-MDBT, and 4,6-DMDBT solutions were irradiated with 8W UV light (254 nm). The amount of degradation of BT in solution was measured by GC-FID after 0.25, 0.75, 1, 1.5, and 2 h of irradiation; for 2-MBT, after 1, 2, 3, 4, 5, and 8 h; for 4,6-DMDBT, after 2, 4, 6, 12, and 14 h; and for DBT and 4-MDBT after 2, 4, 6, 12, 14, and 16 h. The time dependence of the decomposition reaction is shown in **Figure 2-3(b)**. The left axis shows the concentration, with an initial concentration of 0.54 mmol/L, and the right axis shows the percentage of decomposition.

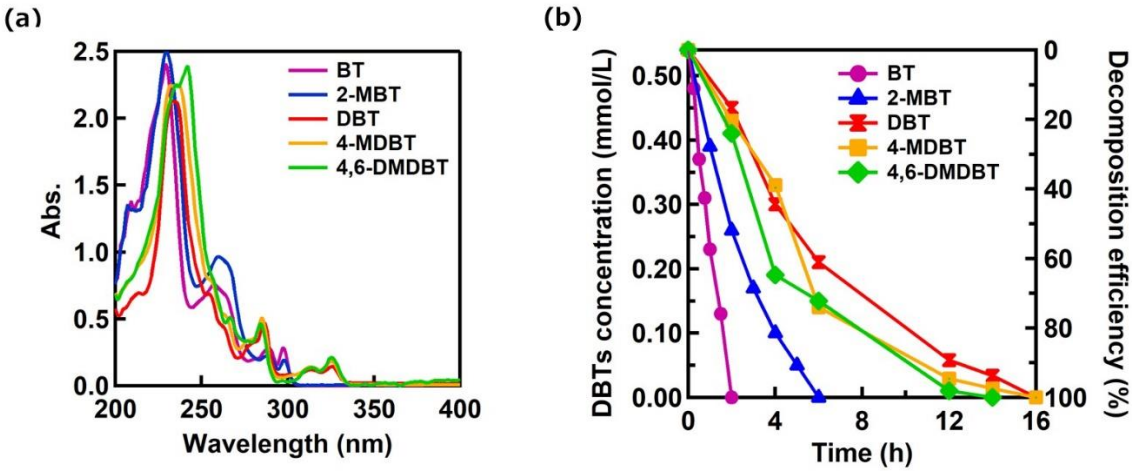

Figure 2-3: (a) UV spectra of BTs and DBTs in cyclohexane; (b) Time dependence of decomposition efficiency and concentration for BTs and DBTs under 8W UV irradiation (254 nm).

The decomposition of BT and 2-MBT reached 100 % in 2 h and 8 h, respectively. In addition, the decomposition of 4,6-DMDBT reached 100 % in 14 h, whereas that of DBT and 4-MDBT reached 100 % in 16 h, i.e., DBT molecules bearing more substituents decomposed faster. This trend is opposite to that is observed in hydrodesulfurization, wherein the desulfurization rate is significantly reduced by the substitution of alkyl groups. This is because the hydrodesulfurization process involving a catalyst to create an intermediate is considerably affected by steric hindrance, whereas under the conditions of photoreaction, which does not require a catalyst, the effect of increasing the electron density by an alkyl substituent is large. Note that when this photodecomposition reaction with UV light was performed under an inert gas atmosphere, the reaction did not proceed at all. This implies that oxygen is involved in the photodecomposition reaction. These results suggest that the reaction is effective for aromatic sulfur compounds with large steric hindrance, which is particularly difficult to achieve with conventional methods; additionally, the ultra-deep desulfurization can be performed more conveniently compared with hydrodesulfurization.

2-3 X-ray fluorescence (XRF) analysis of precipitates

When BTs and DBTs were irradiated with 8 W UV light (254 nm), yellow precipitates were deposited over time at the bottom of the cell (**Figure 2-4(a)**). The precipitates were presumed to be derived from BTs and DBTs, and the X-ray fluorescence (XRF) analysis of the yellow precipitates were performed. The results are shown in **Figures 2-4(b)–(f)**.

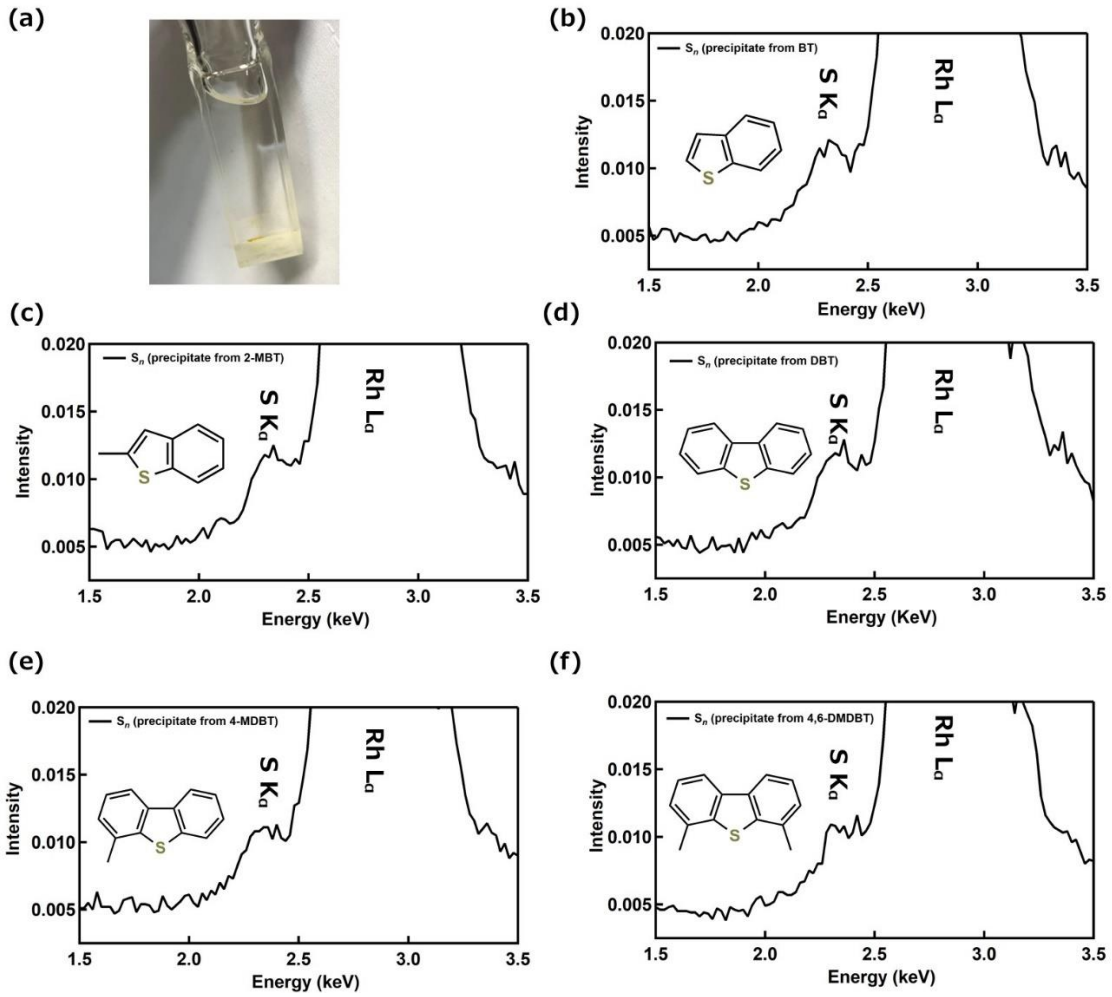

Figure 2-4: (a) Yellow precipitates after UV irradiation of BT and DBT. XRF spectroscopy of yellow precipitates from (b) BT, (c) 2-MB, (d) DBT, (e) 4-MDBT, and (f) 4,6-DMDBT.

The horizontal axis represents the energy (keV) and the vertical axis represents the intensity of the characteristic X-ray. The large peak at 2.5–3.5 keV corresponded to the Rh L_α line originating

from the Rh tube as the primary X-ray source, whereas that at 2.3 keV corresponded to the sulfur K_α line. In all the spectra of **Figures 2-4(b)–(f)**, the characteristic X-ray peak of sulfur K_α was observed. These results suggest that the yellow precipitates contained sulfur atoms. The precipitates were assumed to be sulfur atom and its allotropes derived from BTs and DBTs.

2-4 Characterization of the yellow precipitates by high-performance liquid chromatography (HPLC) and atmospheric pressure solid analysis probe-mass spectrometry (ASAP-MS)

The yellow precipitates produced by UV irradiation of BTs and DBTs were analyzed by high-performance liquid chromatography (HPLC), and a single peak was detected at around 10 min (**Figures 2-5(a)–(e), red line**). Next, standard sulfur was analyzed similarly, and a peak of the same shape was detected at around 10 min (**Figures 2-5(a)–(e), yellow line**). In addition, when these two samples were injected simultaneously, the peaks overlapped completely (**Figures 2-5(a)–(e), blue line**). Meanwhile, the retention time for BTs, DBTs and low polarity sulfur compounds under the same HPLC conditions was much shorter (2–5 min), which is not consistent with the yellow precipitates (**Figure 2-6**).

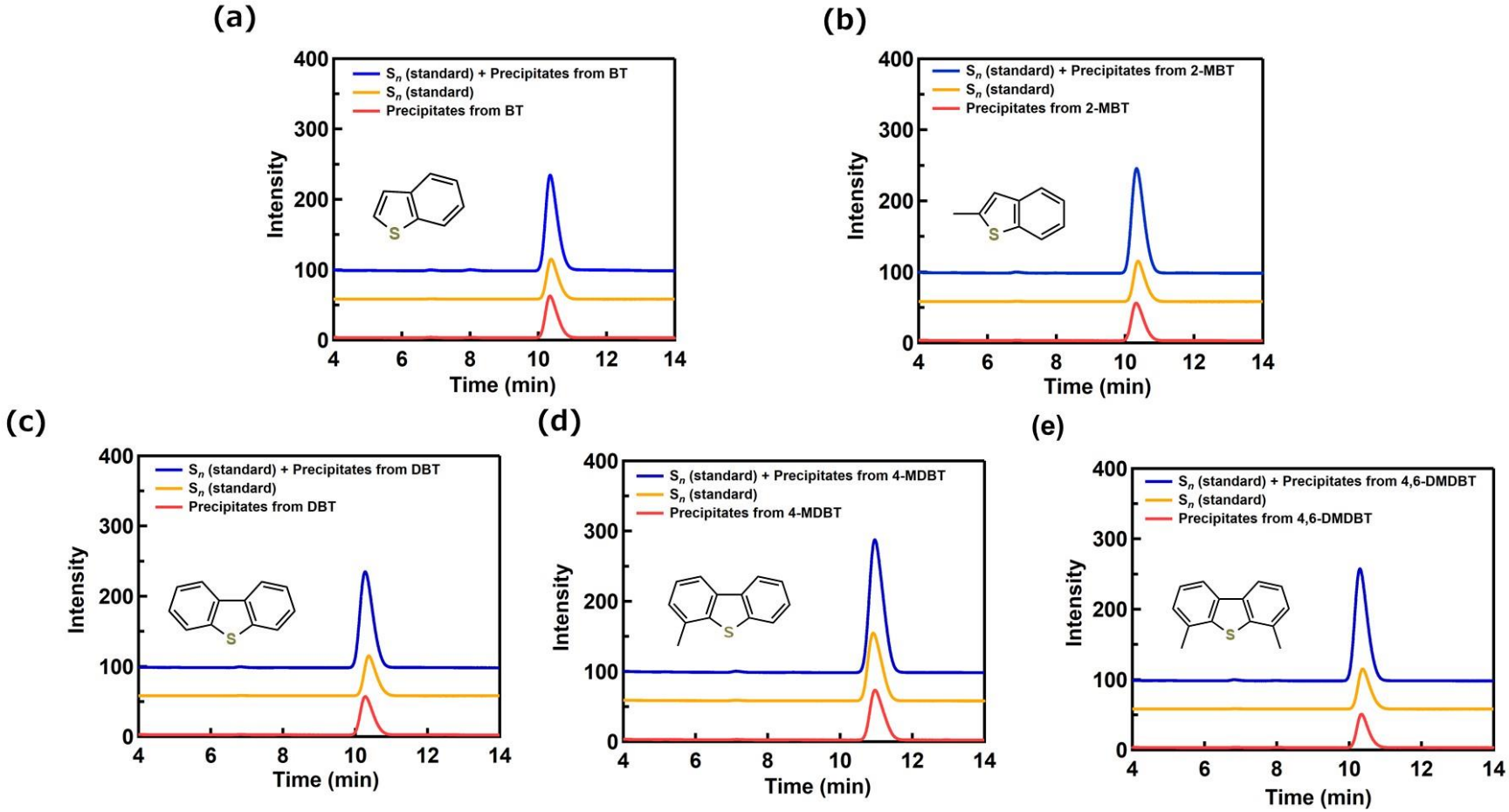

Figure 2-5: HPLC chromatograms of the precipitates (a) after UV irradiation of BT, (b) after UV irradiation of 2-MBT, (c) after UV irradiation of DBT, (d) after UV irradiation of 4-MDBT, and (e) after UV irradiation of 4,6-DMDBT.

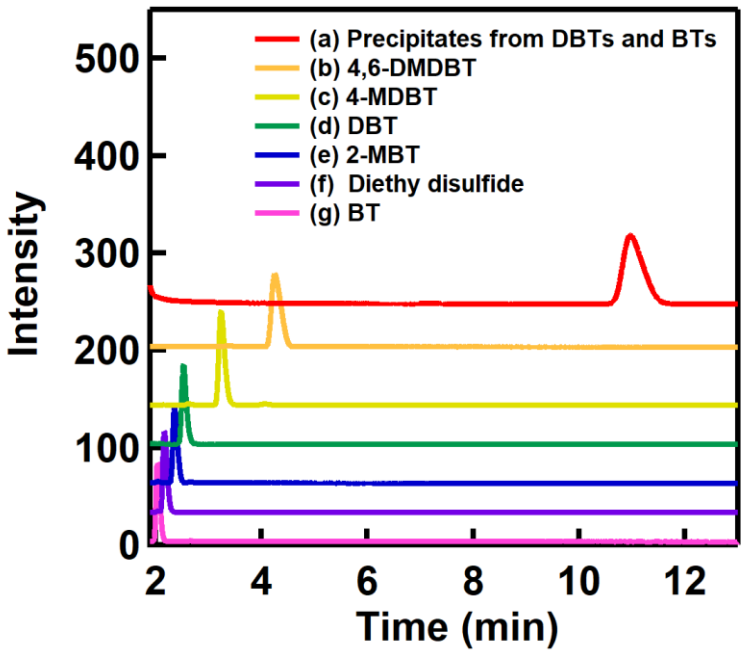

Figure 2-6: HPLC chromatograms of (a) yellow precipitates after 8W UV irradiation (254 nm) of BTs and DBTs, (b) 4,6-DMDBT (standard), (c) 4-MDBT (synthesis), (d) DBT (standard), (e) 2-MBT (standard), (f) Diethyl disulfide (standard), and (g) BT (standard).

Next, the yellow precipitates were analyzed by mass spectrometry using atmospheric pressure solid analysis probe-mass spectrometry (ASAP-MS), which is direct injection mass spectrometry at atmospheric pressure. Standard sulfur was measured, and fragment ions of allotropes of sulfur (S_n) with m/z = 256 (S_8^+), 224 (S_7^+), 192 (S_6^+), 160 (S_5^+) and 128 (S_4^+) were detected (**Figure 2-7**). Similarly, the yellow precipitates were analyzed and fragment ions with m/z = 256 (S_8^+) and 224 (S_7^+) were detected (**Figure 2-8**). These results indicates that the yellow precipitates after UV irradiation was S_8 or a mixture of its allotropes (S_n). Consequently, XRF, HPLC, and ASAP-MS analyses revealed that the yellow precipitates were either single sulfur or its allotropes, thus indicating that only sulfur atom was removed by desulfurization using UV irradiation.

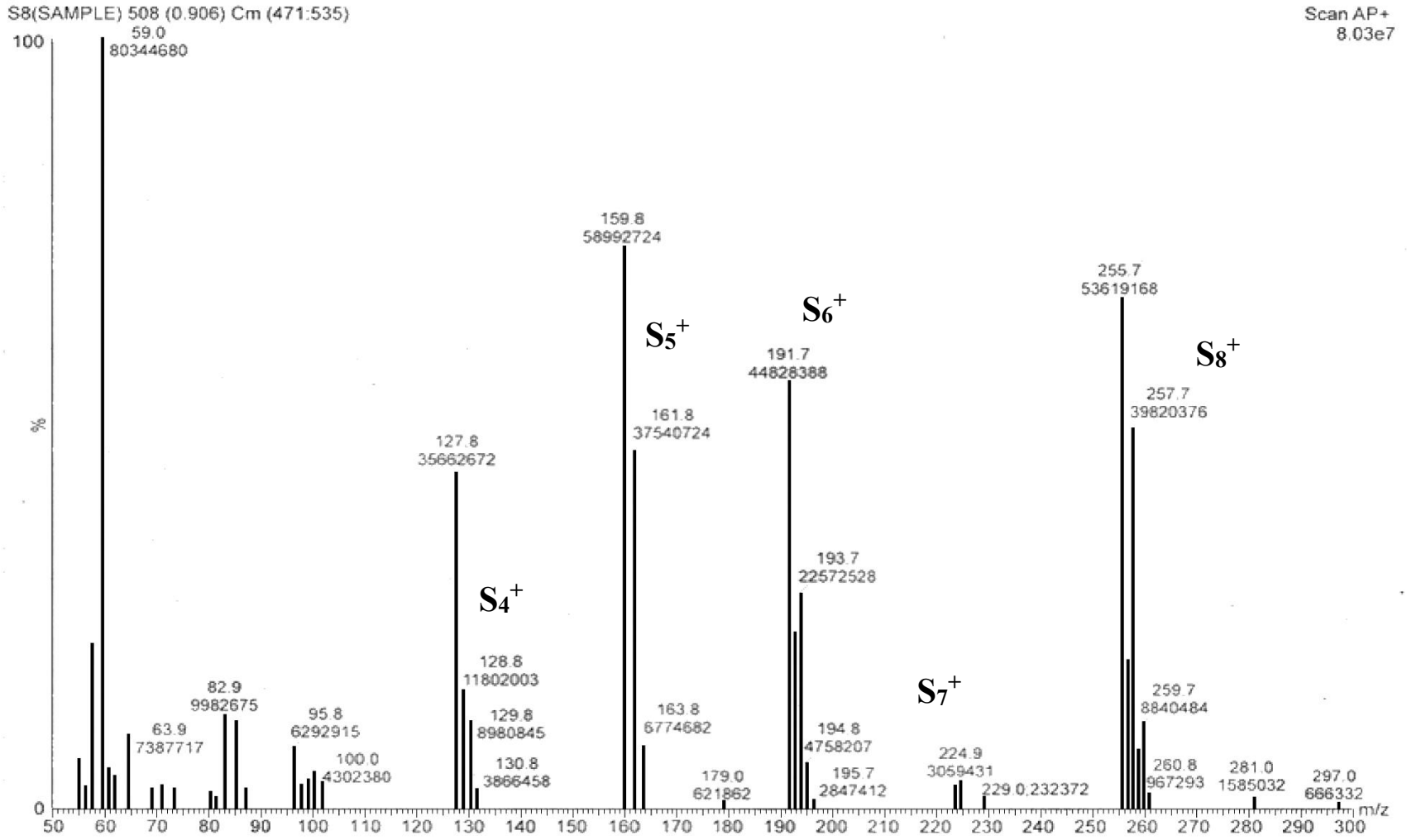

Figure 2-7: ASAP-MS spectrum for sulfur (standard).

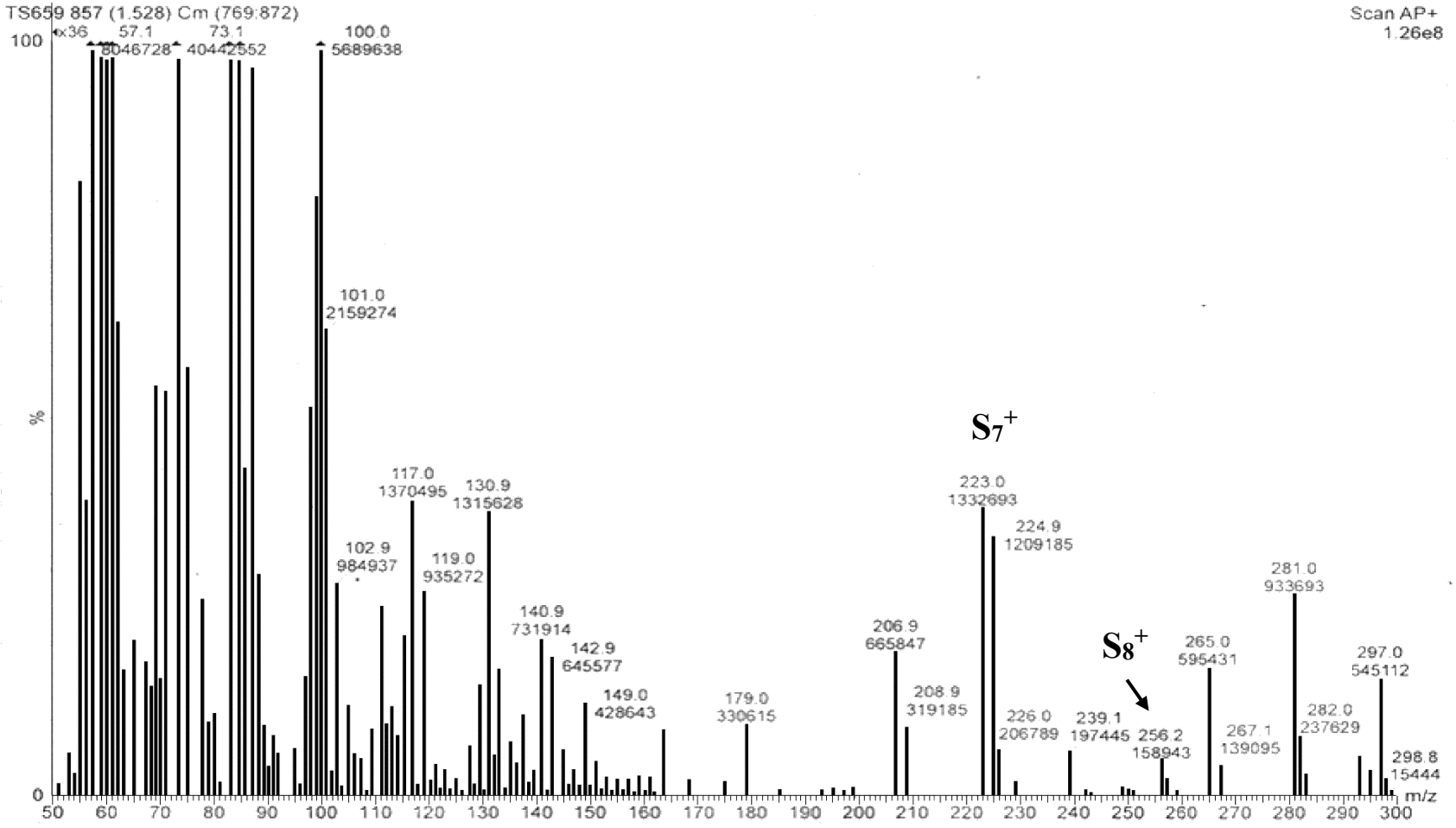

Figure 2-8 ASAP-MS spectrum for precipitates after 8W UV (254 nm) irradiation (24 h) of BTs and DBTs.

2-5 Quantitative analysis of yellow precipitates produced by UV irradiation

To determine the amount of precipitated sulfur, the relationship between the XRF peak intensity and amount of sulfur was investigated. Standard solutions of sulfur were prepared at concentrations of 50, 100, and 200 mg(S)/L (25, 50, and 100 µg S per 0.5 mL). A calibration curve was constructed based on the detected signal intensity of S K_α at 2.3 keV, and good linearity was obtained. (**Figure 2-9**). After 8W UV irradiation (254 nm), the reaction mixture was concentrated, the resulting yellow precipitates were dissolved in 0.5 mL of acetone, and the entire amount was impregnated in filter paper (φ21 mm) to prepare a sample for XRF measurement. The yields were calculated based on the observed signal intensity of S K_α (**Table 2-1**). The calculated values were 79–95 %, which is reasonably close to 100 % for analysis of a micro-scale reaction. Accordingly, almost all the sulfur atoms in BTs and DBTs were expected to be converted into sulfur atom, S_8, or a mixture of its allotropes (S_n).

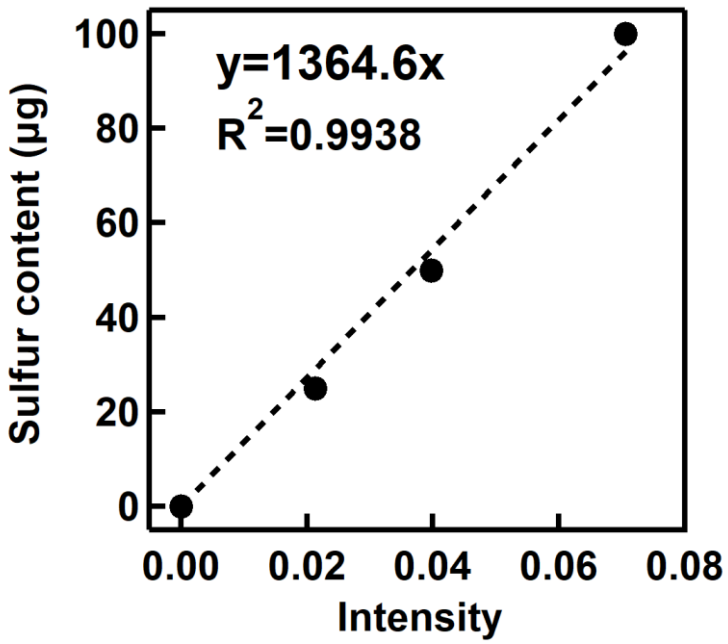

Figure 2-9: Calibration curve of sulfur.

Table 2-1: Yield of allotropes of sulfur (S_n) during UV irradiation of BTs and DBTs by XRF.[a]

Compound	Intensity	Weight (μg)	Yield (%)[b]
BT	0.034	46	88
2-MBT	0.036	49	95
DBT	0.034	46	88
4-MDBT	0.030	41	79
4,6-DMDBT	0.034	46	88

[a] After 24 h of 8W UV irradiation (254 nm).

[b] Yield = BTs and DBTs conc. (mg/L) × quartz cell volume (L) × 1/(BTs or DBT MW) × 1/8 × Sulfur MW.

2-6 Photodecomposition of deuterium-labeled DBT-d_8

Thus far, focus was placed on the behavior of sulfur and have shown that sulfur atoms in BTs and DBTs are converted into sulfur atom. Next, the ways in which the hydrocarbon moiety of these compounds changes during photodecomposition were investigated using GC-MS. With cyclohexane as the solvent, the decomposed products from BTs and DBTs with a boiling point lower than that of cyclohexane (80.7 °C) could overlap with cyclohexane in the chromatogram. Hence, *trans*-decalin, which has a higher boiling point (190 °C), was chosen as the solvent instead of cyclohexane. A 0.54 mmol/L DBT solution was irradiated with UV light for 24 h and the irradiated solution was analyzed by GC-MS. As a result, a trace amount peak was observed at 2.9 min (**Figure 2-10(a)**. When the mass spectrum of the peak detected at 2.9 min was analyzed, fragment ions (*m/z* = 78, 77, 51) presumed to be benzene were detected (**Figure 2-10(b)**); these fragment ions were assumed to be similar to the fragment ions for benzene. When benzene (standard) was measured by GC-MS, a GC peak was detected at 2.9 min and similar fragment

ions (*m/z* = 78, 77, 51) were detected. To confirm whether the produced benzene was derived from DBT, a decomposition experiment was conducted using deuterated DBT (DBT-d_8). The solution containing DBT-d_8 was irradiated with UV light for 24 h, and the irradiated solution was measured by GC-MS. Again, a GC peak was detected with a retention time of 2.9 min, and the mass spectrum exhibited fragment ions (*m/z* = 82, 81, 55), presumed to be benzene-d_4 (**Figures 2-10(c) and (d)**). The detected benzene is thought to be derived from the carbon and hydrogen atoms adjacent to the sulfur atom of the substrate DBT. Therefore, the author confirm for the first time that benzene was formed as one of the decomposition products from the decomposition of DBT by UV irradiation.

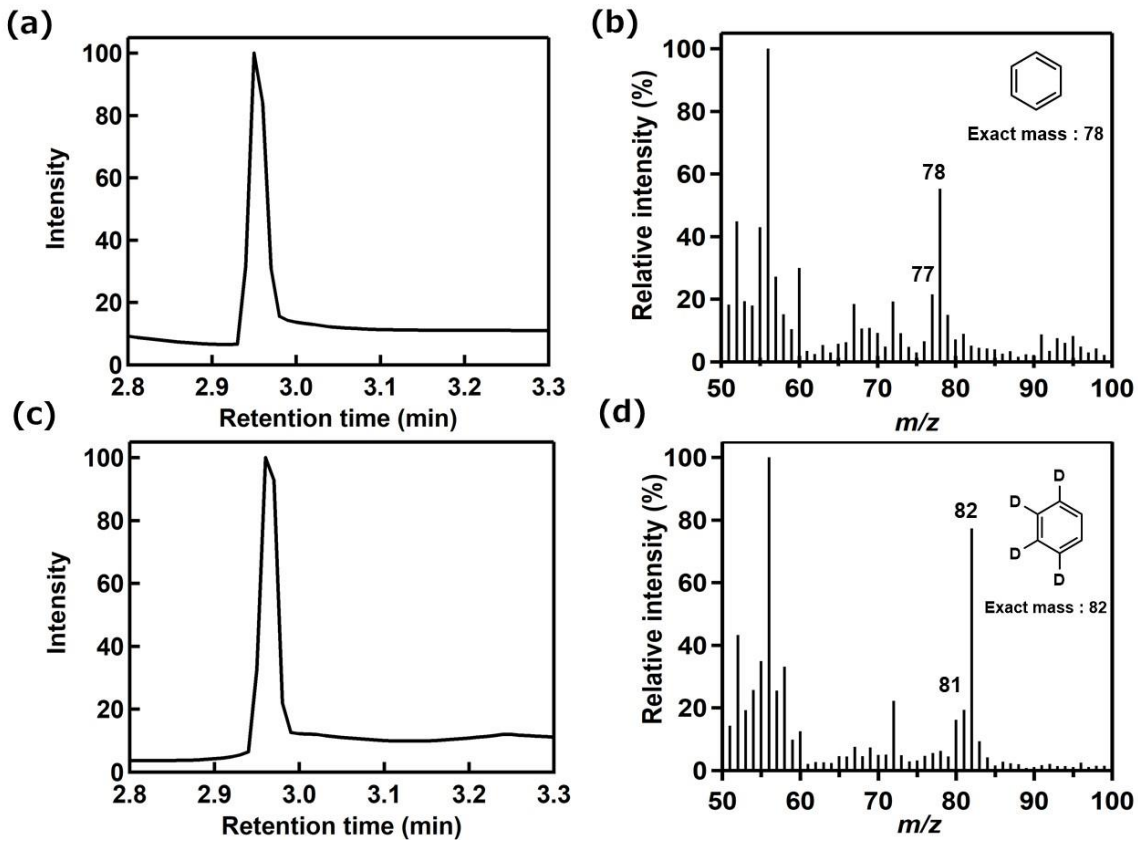

Figure 2-10: (a) Chromatograph obtained from GC-MS after 8 W UV irradiation (254 nm) of DBT solution; (b) Mass spectrum after 8 W UV irradiation (254 nm) of DBT solution

(SIM mode); (c) Chromatograph obtained from GC-MS after 8 W UV irradiation (254 nm) of DBT-d_8 solution; (d) Mass spectrum after 8 W UV irradiation (254 nm) of DBT-d_8 solution (SIM mode).

2-7 Desulfurization of high-concentration sulfur solution

As mentioned in the introduction, recent regulations have led to the distribution of fuels containing low concentrations (<10 mg(S)/L) of sulfur; however, in numerous regions, fuels containing high concentrations of sulfur are still supplied (>100 mg(S)/L). Therefore, the usefulness of the degradation by UV irradiation in solutions containing high concentrations of sulfur was investigated. BTs and DBTs were dissolved in cyclohexane to obtain solutions with a sulfur concentration of 100 mg(S)/L (3.1 mmol/L) and irradiated with 8W UV light (254 nm). The total sulfur concentration was reduced to 50 mg(S)/L (1.56 mmol/L) in 24 h; however, no significant change in concentration was observed thereafter (**Figure 2-11(a), left axis, bar graph**). Furthermore, after 24 h, the decrease in the BT or DBT concentration was negligible **(Figure. 2-11(a), right axis, line graph).** Presumably, the sulfur generated when BTs and DBTs are irradiated with UV light could absorb light and inhibit decomposition. Therefore, the suspended and precipitated sulfur was separated and removed by centrifuging every 24 h, and the solution was irradiated with UV light again. In this case, the sulfur concentration after 60 h decreased to 7 mg(S)/L (0.21 mmol/L), and ultra-deep desulfurization (<10 mg(S)/L) was achieved **(Figure 2-11(b), left axis, bar graph)**. In addition, the sulfur concentration (mg/L) of each BT and DBT compound decreased with time **(Figure 2-11(b), right axis, line graph)**. Accordingly, this method is useful for solutions containing high concentrations of sulfur, and ultra-deep desulfurization can be performed easily.

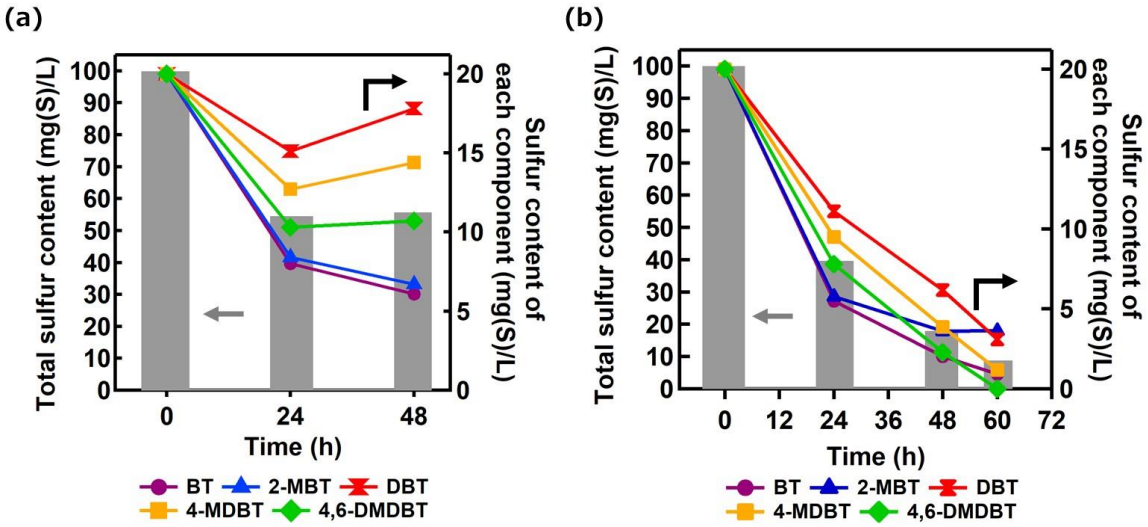

Figure 2-11: Desulfurization efficiency of high-concentration sulfur solutions using UV light (a) without centrifugation and (b) with centrifugation.

2-8 UV irradiation of solution containing aromatic compounds

Gasoline and diesel fuel contain a considerable percentage of aromatic compounds. Therefore, it was examined whether this method is also effective for solutions containing a large amount of aromatic compounds. DBT was dissolved in cyclohexane containing 10, 15, or 20% toluene. In addition, DBT was dissolved in gasoline. Each of the prepared solutions was irradiated with UV light for 24 hours (**Table 2-2**).

Table 2-2: Calculation of decomposition efficiency in the presence of aromatic compounds.

Solvent	Degradation efficiency (%)
Cyclohexane (contains 10 % toluene)	72.8
Cyclohexane (contains 15 % toluene)	56.4
Cyclohexane (contains 20 % toluene)	23
Gasoline	6.4

Evidently, the degradation rate of DBT decreased as the concentration of aromatic compounds increased. This suggests that aromatic compounds other than DBT absorb the irradiated UV light and inhibit the decomposition of DBT.

2-9 Pseudo-first-order plot for the degradation of BTs and DBTs

The decomposition reaction using UV light irradiation has not been extensively investigated, and only few studies on reaction kinetics have been reported. Thus, kinetic experiments were conducted in this study to examine the rate dependence on the substrate structure and obtain some mechanistic insight. The initial concentrations of BTs and DBT were 0.54 mmol/L, and the progress of the reactions under UV irradiation was monitored by GC-FID analysis with frequent sampling. When the photodecomposition reaction of DBT was performed under N_2 (in the absence of O_2), the reaction did not proceed at all. This confirms that O_2 is involved in the reaction. When the reaction was performed in air, the amount of oxygen in the quartz cell was sufficient for degradation to proceed. The dissolved oxygen was calculated to be approximately 15 mmol/L, which is more than 20 times higher than the concentrations of BT and DBT (0.54 mmol/L). Consequently, under these conditions, the oxygen concentration can be considered constant during the reaction, and the decomposition rate constants k_{obs} for BTs and DBTs were calculated from equation (1), assuming a pseudo-first-order reaction.

$$-\frac{d[\text{DBTs or BTs}]}{dt} = k[\text{DBTs or BTs}][O_2] \approx k'[\text{DBTs or BTs}], \quad (1)$$

$$-\ln\frac{[\text{DBTs or BTs}]_t}{[\text{DBTs or BTs}]_0} = k_{\text{obs}}t, \quad (2)$$

Where $[DBTs \text{ or } BTs]_0$ and $[DBTs \text{ or } BTs]_t$ represent the concentrations of BTs and DBTs before and after UV irradiation at time *t*, respectively (**Table 2-3, Figure 2-12**).

Table 2-3: Rate constants for UV irradiation of BTs and DBTs.

Compound	k_{obs} (h^{-1})	*v* (mmol/L·h)
BT	0.954	0.515
2-MBT	0.427	0.231
DBT	0.202	0.109
4-MDBT	0.269	0.145
4,6-DMDBT	0.315	0.170

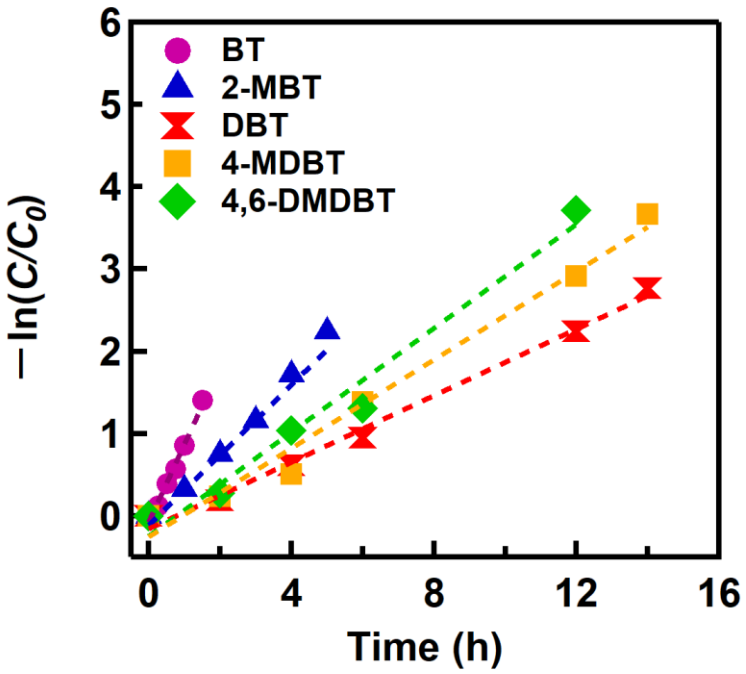

Figure 2-12: Pseudo-first-order kinetics for degradation of BTs and DBTs.

The pseudo-first order plot for each experiment revealed good linearity for up to two half-lives for BT and over three half-lives for the other substrates. The decomposition rate constants k_{obs} were calculated from the slope of the line and were 0.954, 0.427, 0.202, 0.269, and 0.315 h^{-1} for BT, 2-MBT, DBT, 4-MDBT, and 4,6-DMDBT, respectively; the reaction rates v were 0.5, 0.22, 0.11, 0.14, and 0.16 mmol/L·h, respectively. BTs decomposed faster than DBTs, and a methyl substituent on the thiophene ring reduced the reaction rate by half. Conversely, methyl substituents on the benzene ring of DBT slightly accelerated the reaction. The results of the kinetic experiments obtained with DBT exhibit a clear difference from catalytic reactions, where steric hindrance decreases the reaction rate.

2-10 Possible reaction mechanism of degradation of BTs and DBTs by DFT calculation

The UV-light-induced decomposition of DBT, 4-MDBT, and 4,6-DMDBT were studied theoretically. All calculations were performed using Gaussian 16[1] and GAMESS (2020 R2) software[2], and the results were visualized with GaussView and Facio[3-4]. First, the photochemical path of sulfur extrusion was elucidated from DBTO, the previously proposed reaction confirmed in our photodegradation experiment of DBTO. The geometries of all the ground and excited species involved in the reactions were fully optimized using the Spin-Flip TDDFT (BHHLYP/6-31G**) method implemented in GAMESS. The calculated energy profile is summarized in **Figure 2-13.** First, the two transition states TS1 and TS2, the expected transition states of DBTO to dibenzo[*c*,*e*]oxathiine (DBSO) and of (*Z*)-6'-thioxo-[1,1'-bi(cyclohexylidene)]-2',3,4',5-tetraen-2-one (DBSXO) to 1a*H*-benzo[*b*]thiireno[2,3-*h*]benzofuran (dibenzofuran episulfide, DBFES), respectively, were located. The former was successfully located. Identification of the latter was unsuccessful using Spin-Flip TDDFT but successful using Gaussian 16 (B3LYP/6-31G*) (**Figure 2-14**).

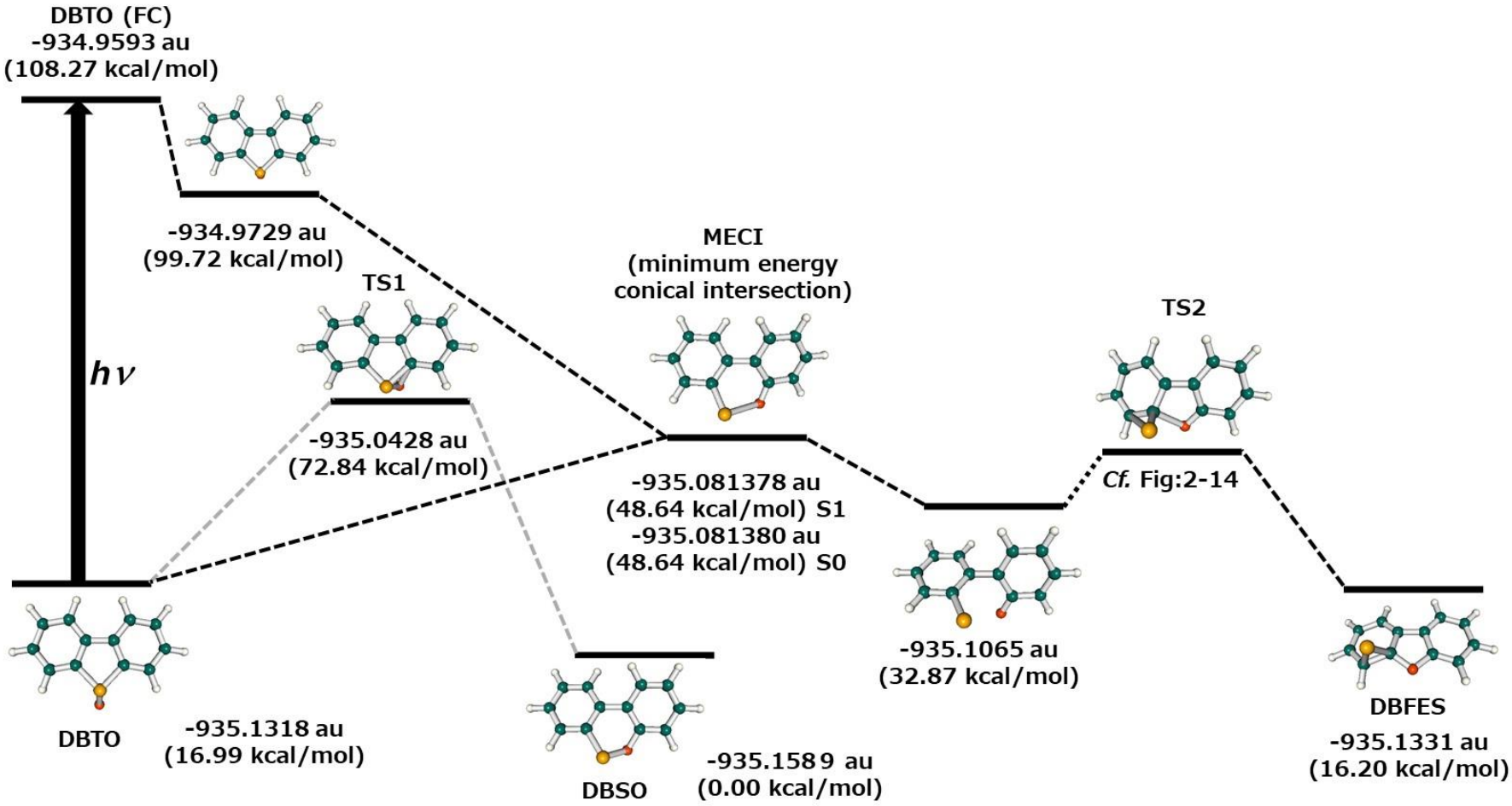

Figure 2-13. Energy profile of the photochemical path of sulfur extrusion from DBTO.

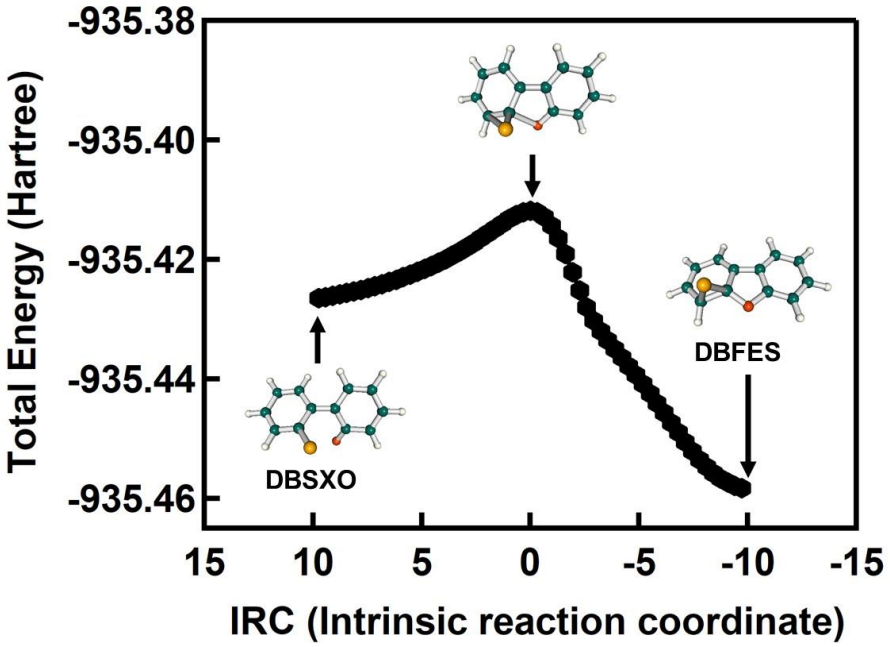

Figure 2-14. TS2, transition state of DBSXO to DBFES (dibenzofuran episulfide).

Although TS1 was located, a thermal reaction path through this transition state seems almost impossible because the activation energy for TS1 is 55.85 kcal/mol. Therefore, the photoreaction pathway was studied. Using the optimized structure of the ground state DBTO, the energy of the Franck-Condon state was calculated, and subsequently, the geometry of the singlet excited state was optimized. Starting from the optimized DBTO(S1), the minimum energy conical intersection (MECI) was successfully located. Given that the S–O bond distance of the MECI was 2.64 Å, substantially longer than that of DBTO (1.68 Å), cleavage of the S–O bond should be easy and the MECI seems to be transformed to DBSXO, which could be thermally transformed to DBFES, as shown in **Figure 2-14**. However, the excitation step is probably not a rate-determining step as the reaction rate measurement revealed that the UV-light-induced decomposition of DBT was pseudo-first order. Consequently, the author turned our attention to the formation of DBTO.

For all the calculations related to DBTO formation, Gaussian 16 (B3LYP/6-31+G**) was used.

First, a complex of DBT and O_2 was determined, and an DBT-O_2 (σ-complex) was discovered (**Figure 2-15**).

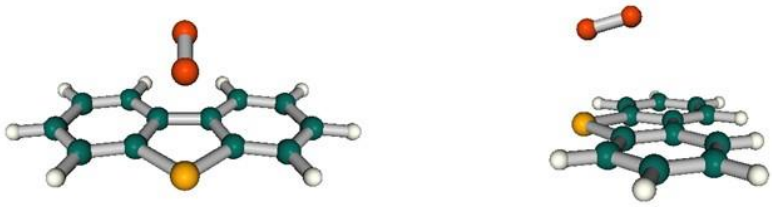

Figure 2-15. DBT-O_2 (σ-complex).

Next, the reaction of DBT-O_2 (σ-complex) and DBT was examined, and a transition state was found. Intrinsic reaction coordinate (IRC) calculation confirmed that the transition state was formed from the starting materials and could be transformed to two molecules of DBTO (**Figure 2-16**). Based on this result, further calculations were performed on other DBTs (4-MDBT and 4,6-DMDBT) to locate their respective transition states.

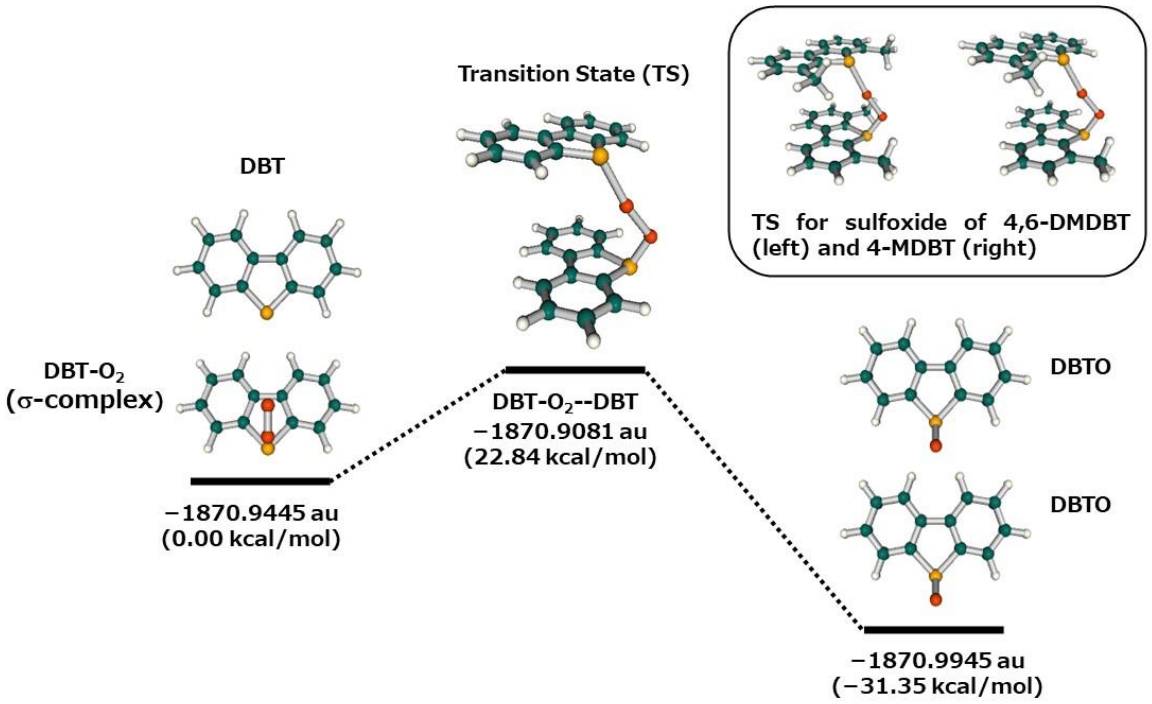

Figure 2-16: Reaction pathway from DBT and DBT-O_2 (σ-complex) to two DBTO molecules via transition states.

The shape of the lowest unoccupied molecular orbital (LUMO) of DBT-O_2 (σ-complex) depicted in **Figure 2-17** revealed that its lobes exist predominantly near oxygen atoms with an anti-bonding feature, and therefore, the type of reaction illustrated in **Figure 2-16** could be feasible.

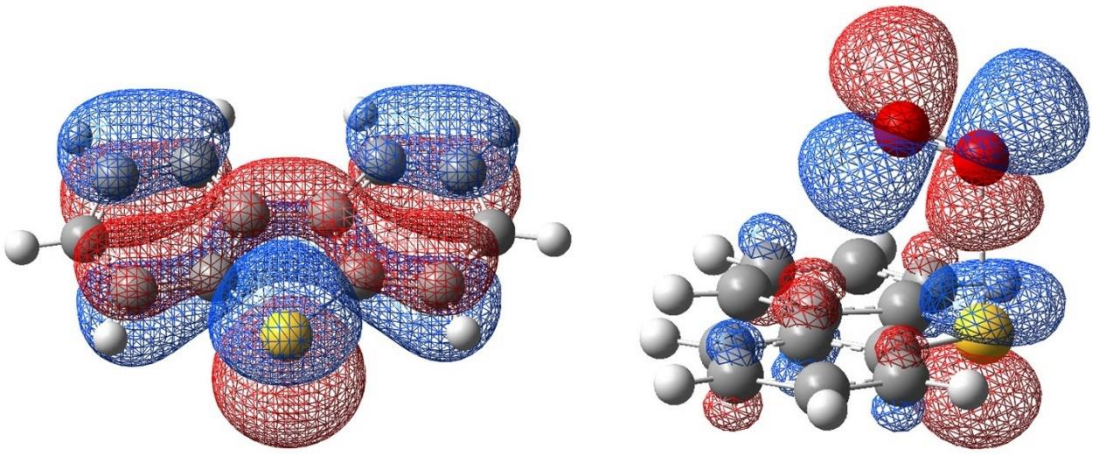

Figure 2-17: HOMO of DBT and LUMO of DBT-O_2 (σ-complex).

Using the transition states of three DBTs, the difference in their reaction rates were attributed to the difference in their activation energies. The HOMO-LUMO gaps listed in **Table 2-4** suggested that the reaction rates increased in the order DBT < 4-MDBT < 4,6-DMDBT. However, a comparison of the activation energies revealed that they were all nearly equal, as listed in **Table 2-5**. Thus, the differences in the activation energies could not account for the differences in reaction rates**.** Therefore, the formation of DBTO was reinvestigated.

Table 2-4: MO energies HOMO of DBTs, LUMO of DBT-O_2 (σ-complex) and their difference.

Compound	**HOMO (au)**	**Compound**	**LUMO (au)**	**LUMO – HOMO (au)**
DBT	−0.2232	DBT-O_2	−0.1411	−0.0821
4-MDBT	−0.2206	4-MDBT-O_2	−0.1413	−0.0793
4,6-DMDBT	−0.2183	4,6-DMDBT-O_2	−0.1403	−0.0780

Table 2-5: Activation energies for transition state DBT-O_2 (σ-complex)—DBTs.

	DBTs (au)	**DBTs-O_2 (au)**	**DBTs-O_2-DBTs (au)**	**Activation energy (kcal/mol)**
DBT	–860.3360	–1010.6085	–1870.9081	22.84
4-MDBT	–899.6581	–1049.9315	–1949.5530	22.97
4,6-DMDBT	–938.9801	–1089.2537	–2028.1984	22.21

Previous studies that DBT is known to react with O_2 by the Diels–Alder reaction to form thiadioxolane (DBTDX, 4a,6a-epithiodibenzo[*c*,*e*][1,2]dioxine), as shown in **Figure 2-18**[5-6].

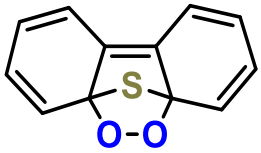

Figure 2-18: Diels-Alder product of DBT and O_2.

Optimization of the dimeric structure of DBTDX with different initial S–S bond lengths revealed a significant difference. In the case of a bond length of 2.87 Å, an optimized dimer formed, and the initial dimeric structure was unexpectedly transformed to two molecules of DBDX (dibenzo[*c*,*e*][1,2]dioxine), accompanied by extrusion of diatomic sulfur, S_2, as shown in **Scheme 5**.

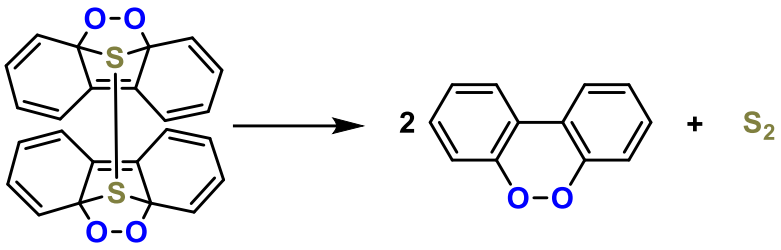

Scheme 5: Extrusion of S_2 from DBTDX dimer.

As is well-known, sulfur loss proceeds through a lower energy transient species, such as diatomic sulfur or longer chain fragments. Thus, sulfur extrusion can occur directly without proceeding through DBTO, unlike the common notion.

Encouraged by this result, the transition state for DBTDX formation was located. Using the zero temperature string method implemented in NWChem[7], an initial structure of transition state calculation was obtained, as shown in **Figure 2-18** and optimized with Gaussian 16.

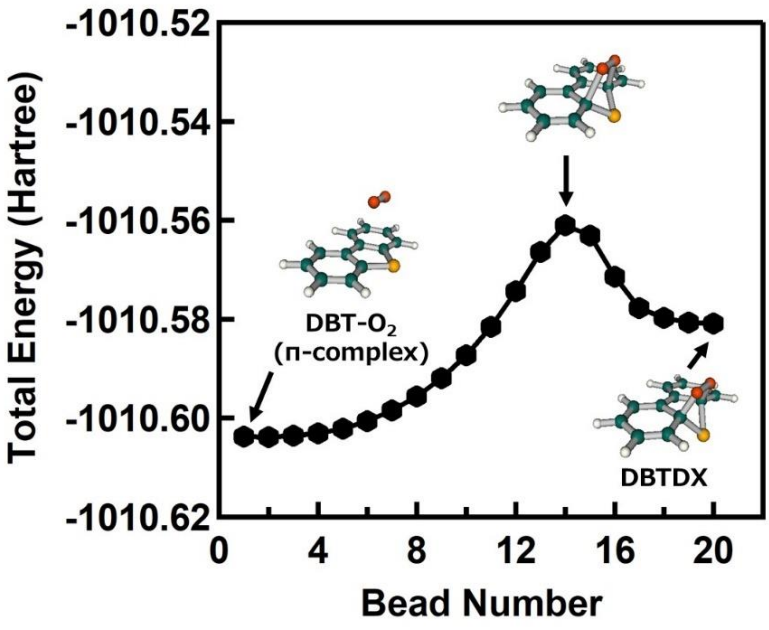

Figure 2-18. Estimated transition state for DBTDX by the Zero Temperature String Method of NWChem.

Considering the activation energy to DBTDX is 26.30 kcal/mol, its occurrence is possible. Considering the activation energy for dimerization (estimated by optimization of the dimer to be approximately 40 kcal/mol), it was expected to occur thermally. Although the evidence is lacking at this stage, the author assumed that the excited triplet state of DBTDX participates in the dimerization.

The transition state of the Diels–Alder reaction for other DBTs was obtained in a similar manner. With the transition state, the calculated activation energies (from ground state DBTs + ground state triplet O_2 to transition states) were 63.19, 62.14, and 61.35 kcal/mol for DBT, 4-MDBT, 4,6-DMDBT, respectively. Although this result suggests the reaction rate order was DBT < 4-MDBT < 4,6-DMDBT, in agreement with our experimental results, the occurrence of the Diels–Alder reaction is impossible considering the large activation energies. Consequently, the DBT-O_2 complex was considered. The leftmost structure in **Figure 2-18** was optimized using Gaussian 16, and another DBT-O_2 complex, in which O_2 forms a π-complex with the thiophene ring, was obtained. This π-complex has an energy that is 2.30 kcal/mol higher than that of the σ-complex (**Figure 2-19**).

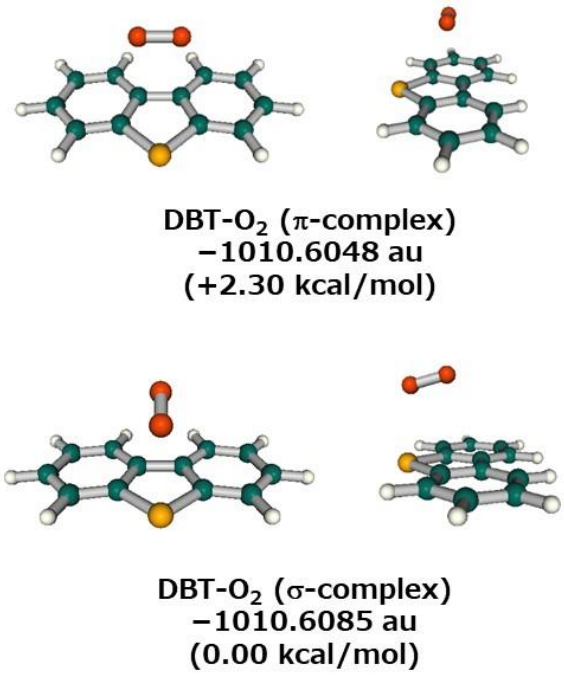

Figure 2-19: Two types of isomers for DBT and O_2 complex.

First, a DBT-O_2 (π-complex) was formed by photoactivation and not by thermal activation as the energy difference between DBTs + triplet O_2 and DBTs-O_2 (π-complex) was approximately 37 kcal/mol. The excited triplet state of the DBTs were calculated with Spin-Flip TDDFT (B3LYP/6-31+G**), and the determined energy differences between excited triplet DBTs + triplet O_2 and DBTs-O_2 (π-complex) were 270.41, 290.39 and 308.74 kcal/mol for DBT, 4-MDBT, and 4,6-DMDBT, respectively. These results indicate that the exothermic amounts increased in the same order, and if Hammond's postulate of photochemical reactions could be applied, the reaction rate was presumed to increase accordingly. The author consider this to be the origin of the difference. As the energy difference between the ground state (DBTs + O_2) and the DBTs-O_2 (π-complex) were almost identical (*ca*. 36 kcal/mol), the exothermic amount could be attributed to the difference between the ground state energy and excited triplet state energy of the DBTs.

Based on the theoretical calculations described above, the complete reaction is summarized in

Figure 2-20. First, the photoactivated DBTs reacted with O_2 to form DBTs-O_2 (π-complex), which isomerized to a more stable DBTs-O_2 (σ-complex). Next, the σ-complex reacted with DBTs to form DBTOs. Subsequently, the DBTOs were photoactivated and transformed to DBFES, from which extrusion of a sulfur atom occurred, as outlined in **Figure 2-20.**

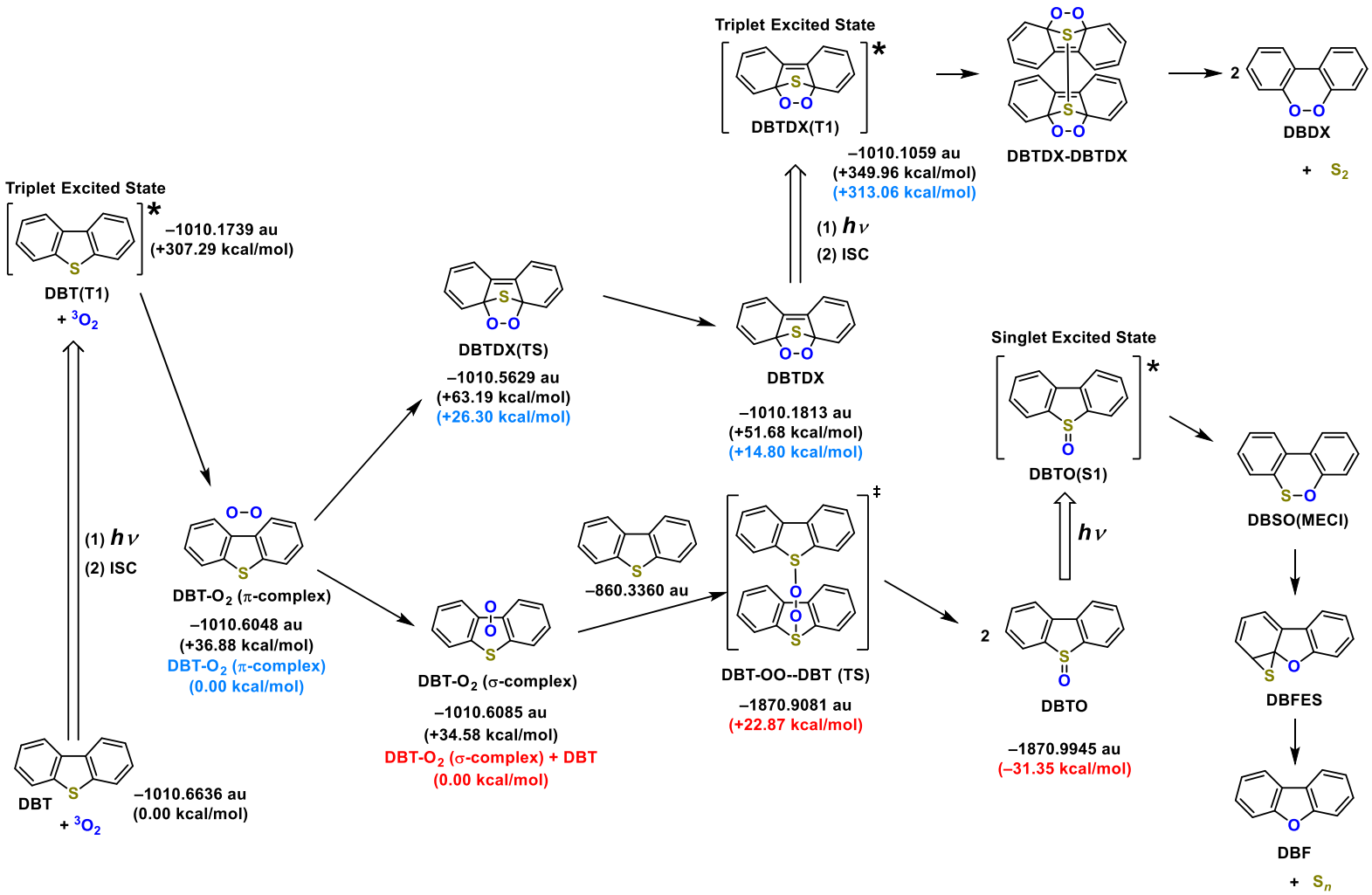

Figure 2-20. Proposed reaction paths and energy profiles;energy values in brackets are relative to [DBT + $^3O_2$] (in black), [DBT-O_2 (σ-complex) + DBT] (in red), and [DBT-O_2 (π-complex)] (in blue).

Finally, the formation of byproducts was studied. The DBTs-O_2 (σ-complex) were considered to be photochemically activated to a singlet excited state, followed by intersystem crossing to give a triplet excited state. Therefore, the DBTs-O_2 (σ-complex) could be a relevant active species that abstracts hydrogen atoms from a solvent (cyclohexane) to produce radical species, such as cyclohexyl radical and DBT-OOH radical (**Figure 2-21**). As another possible reaction route, DBT-OOH radical itself could decompose to produce DBTO and hydroxyl radical. Subsequently hydroxyl radical would react with the cyclohexyl radical to produce cyclohexanol and abstract a hydrogen atom from the resulting cyclohexanol to give a corresponding radical. This radical could react further with cyclohexyl or a hydroxy group present in the solvent to form dicyclohexyl ether or cyclohexanone as byproducts.

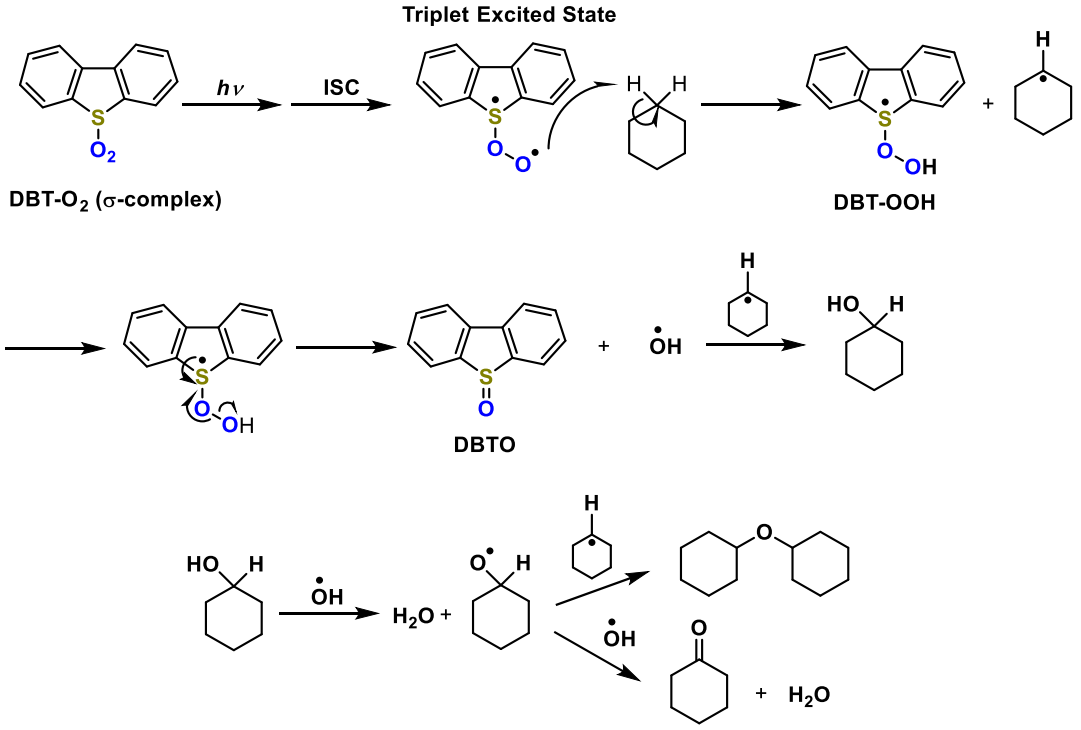

Figure 2-21. Proposed reaction mechanism for the formation of byproducts and alternative reaction route to DBTO.

To confirm the reactivity of the photochemically produced triplet excited state of DBT-O_2 (σ-complex), the spin density was calculated using the TDDFT method with unrestricted B3LYP/6-31+G(d, p). The spin density prevailed at two oxygen and one sulfur atoms is shown in **Figure 2-22**. This suggests that the expected diradical would most likely reside on these atoms, and the proposed reaction scheme in **Figure 2-21** would be feasible.

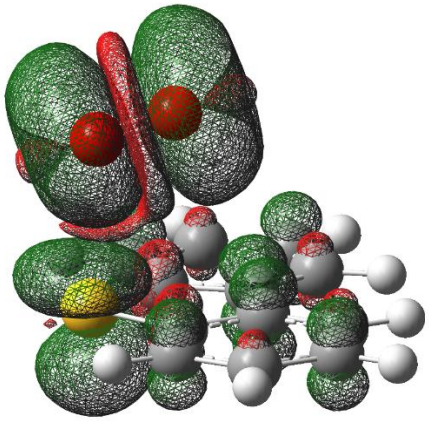

Figure 2-22. Spin density of DBT-O_2 (σ-complex) in the excited triplet state.

3. Conclusion

This study solved the challenging desulfurization of BT, 2-MBT, DBT, 4-MDBT, and 4,6-DMDBT under mild and simple conditions (room temperature, atmospheric pressure, no additives, or catalysts) using UV light. The sulfur atoms in BTs and DBTs were separated as sulfur allotropes (S_n). In addition, identification of the decomposition product of the hydrocarbon part of DBT after sulfur removal suggested that the decomposition proceeded via benzene. Furthermore, the proposed method was effective even in a sample that contained high concentrations of sulfur. When performed with a large excess of oxygen, the method follows a pseudo-first-order reaction. In addition, DFT calculations supported the experimental results obtained. Although further elucidation of the reaction mechanism will be necessary, the complete reaction can be summarized as follows. Photochemically excited triplet DBTs form a complex with $^3O_2$; subsequently, the complex relaxes to become a ground state DBTs-O_2 (π-complex), which isomerizes to DBTs-O_2 (σ-complex). This σ-complex reacts with free DBTs to form two molecules of DBTOs, which again undergo photochemical excitation and transform to the intermediate DBSXO via MECI (**Figure 2-13**), and eventually decompose to extrude sulfur atoms. The rate-determining step of the overall reaction was not identified. However, considering that the energy difference between the complex of triplet excited DBTs + $^3O_2$ and ground state singlet DBTs-O_2 (π-complex) can account for the different reactivities between DBT, 4-MDBT, and 4,6-DMDBT, the rate-determining step is likely related to the formation of the photochemically excited state of DBTs

Reference

1 Frisch, M.J., Trucks, G.W., Schlegel, H.B., Scuseria, G.E., Robb, M.A., Cheeseman, J.R., Scalmani, G., Barone, V., Petersson, G.A., Nakatsuji, H., Li, X., Caricato, M., Marenich, A.V., Bloino, J., Janesko, B.G., Gomperts, R., Mennucci, B., Hratchian, H.P., Ortiz, J.V., Izmaylov, A.F., Sonnenberg, J., Williams-Young, D., Ding, F., Lipparini, F., Egidi, F., Goings, J., Peng, B., Petrone, A., Henderson, T., Ranasinghe, D., Zakrzewski, V. G., Gao, J., Rega, N., Zheng, G., Liang, W., Hada, M., Ehara, M., Toyota, K., Fukuda, R., Hasegawa, J., Ishida, M., Nakajima, T., Honda, Y., Kitao, O., Nakai, H., Vreven, T., Throssell, K., Montgomery, J.A., Peralta, J.J.E., Ogliaro, F., Bearpark, M.J., Heyd, J.J., Brothers, E.N., Kudin, K.N., Staroverov, V. N., Keith, T.A., Kobayashi, R., Normand, J., Raghavachari, K., Rendell, A.P., Burant, J.C., Iyengar, S.S., Tomasi, J., Cossi, M., Millam, J.M., Klene, M., Adamo, C., Cammi, R., Ochterski, J.W., Martin, R.L., Morokuma, K., Farkas, O., Foresman, J.B., Fox, D.J. Gaussian, Inc., Wallingford CT., Gaussian 16, Revision C.01.

2 Barca, G.M.J., Bertoni, C., Carrington, L., Datta, D., Silva, N.D., Deustua, J.E., Fedorov, D.G., Gour, J.R., Gunina, A.O., Guidez, E., Harville, T., Irle, S., Ivanic, J., Kowalski, K., Leang, S.S., Li, H., Li, W., Lutz, J.J., Magoulas, I., Mato, J., Mironov, V., Nakata, H., Pham, B.Q., Piecuch, P., Poole, D., Pruitt, S.R., Rendell, A.P., Roskop, L.B., Ruedenberg, K., Sattasathuchana, T., Schmidt, M.W., Shen, J., Slipchenko, L., Sosonkina, M., Sundriyal, V., Tiwari, A., Vallejo, J.L.G., Westheimer, B., Wtoch, M., Xu, P., Zahariev, F., Gordon, M.S. *J. Chem. Phys.* **2020**, *152*, 154102.

3 Dennington, R., Keith, T.A., Millam, J.M. Semichem Inc., Shawnee Mission, KS, GaussView, Version 6.1.

4 Suenaga, M. Facio: New Computational Chemistry Environment for PC GAMESS. *J. Comput. Chem. Jpn.* **2005**, *4*, 25-32.

5 Suenaga, M. *J. Comput. Chem. Jpn.* **2008**, *7*, 33-54.

6 Sumita, M., Morihashi, K. *J. Phys. Chem. A.* **2015**, *119*, 876-883.

7 Song, X., Fanelli, M.G., Cook, J.M., Bai, F., Parish, C.A. *J. Phys. Chem. A.* **2012**, *116*, 4934-4946.

8 Aprà, E., Bylaska E.J., De Jong, W.A., Govind, N., Kowalski, K., Straatsma, T.P., Valiev, M., Van Dam, H.J.J., Alexeev, Y., Anchell, J., Anisimov, V., Aquino, F.W., Atta-Fynn, R., Autschbach, J., Bauman, N. P., Becca, J.C., Bernholdt, D.E., Bhaskaran-Nair, K., Bogatko, S., Borowski, P., Boschen, J., Brabec, J., Bruner, A., Cauët, E., Chen, Y., Chuev, G.N., Cramer, C.J., Daily, J., Deegan, M.J.O., Dunning Jr., T.H., Dupuis, M., Dyall, K.G., Fann, G.I., Fischer, S.A., Fonari, A., Früchtl, H., Gagliardi, L., Garza, J., Gawande, N., Ghosh, S., Glaesemann, K., Götz, A.W., Hammond, J., Helms, V., Hermes, E.D., Hirao, K., Hirata, S., Jacquelin, M., Jensen, L., Johnson, B.G., Jónsson, H., Kendall, R.A., Klemm, M., Kobayashi, R., Konkov, V., Krishnamoorthy, S., Krishnan, M., Lin, Z., Lins, R.D., Littlefield, R.J., Logsdail, A.J., Lopata, K., Ma, W., Marenich, A.V., Martin del Campo, J., Mejia-Rodriguez, D., Moore, J.E., Mullin, J.M., Nakajima, T., Nascimento, D.R., Nichols, J.A., Nichols, P.J., Nieplocha, J., Otero-de-la-Roza, A., Palmer, B., Panyala, A., Pirojsirikul, T., Peng, B., Peverati, R., Pittner, J., Pollack, L., Richard, R.M., Sadayappan, P., Schatz, G.C., Shelton, W.A., Silverstein, D.W., Smith, D.M.A., Soares, T.A., Song, D., Swart, M., Taylor, H.L., Thomas, G.S., Tipparaju, V., Truhlar, D.G., Tsemekhman, K., Van Voorhis, T., Vázquez-Mayagoitia, Á., Verma, P., Villa, O., Vishnu, A., Vogiatzis, K.D., Wang, D., Weare, J.H., Williamson, M.J., Windus, T.L., Woliński, K., Wong, A.T., Wu, Q., Yang, C., Yu, Q., Zacharias, M., Zhang, Z., Zhao, Y., Harrison, R.J. *J. Chem. Phys.* **2020**, *152*, 184102.

Experimental Section

Analytical instruments

1. Nuclear Magnetic Resonance (NMR)

^{1}H and ^{13}C $\{^{1}H\}$ NMR spectra used a JEOL spectrometer ECA-600 (Tokyo, Japan). Data for ^{1}H NMR spectra were described as follows; chemical shift (δ, ppm), multiplicity (s = singlet, d = doublet, t = triplet and m = multiplet), integration, coupling constants (Hz) and assignment.

2. Gas chromatography-flame ionization detector (GC-FID)

Gas chromatography-flame ionization detector (GC-FID) analysis was performed using an Agilent GC 6850 Series II from Agilent Technologies Corporation (California, USA). Each sample (1 μL) was injected in splitless mode and separated through a J&W HP-1 column (0.25 μm thickness, 0.32 mm I.D., 30 m) and J&W HP-INNOWAX column (0.25 μm thickness, 0.32 mm I.D., 30 m) from Agilent Technologies Corporation (California, USA). The flow rate of nitrogen as carrier gas was 2.0 mL/min. The oven temperature was initially 40 °C. It was ramped to 240 °C at 20 °C/min (5 minutes hold).

3. Gas chromatography-mass spectrometry (GC-MS)

Gas chromatography-mass spectrometry (GC-MS) used a GCMS-QP2010 SE from Shimadzu Corporation (Kyoto, Japan). The ion source temperature and electron energy were 200 °C and 70 eV, respectively. Separated through HP-INNOWAX column (0.25 μm thickness, 0.25 mm I.D., 30 m) from Agilent Technologies Corporation (California, USA). The flow rate of nitrogen as carrier gas was 0.6 mL/min. The oven temperature was initially 40 °C. It was ramped to 120 °C at 5°C/min and increased to 240 °C at 20 °C/min (8 minutes hold). Characteristic ions were determined in full-scan mode at *m/z* 50–150 and single ion monitoring (SIM) mode.

4. X-ray fluorescence (XRF)

Energy dispersive X-ray fluorescence (XRF) spectra measurements were carried out using an EDX-720 XRF from Shimadzu Corporation (Kyoto, Japan). The spectrometer was equipped with a rhodium anode (100 μA of tube current, 50 kV of tube voltage and 50 W of power) and a silicon drift detector. The acquisition time was 100 s. The measurements were performed under air conditions.

5. High performance liquid chromatography (HPLC)

High performance liquid chromatography (HPLC) was performed on a LC-2000 plus series equipped with a variable wavelength detector from JASCO Corporation (Tokyo, Japan) using a XBrige™ prep C_{18} 5 μm, 10 × 150 mm column from Waters (Massachusetts, USA). The mobile phase was acetonitrile/2-propanol/water (40/40/20). The mobile phase flow rate, sample injection volume and detection wavelengths were at 5.0 mL/min, 10 μL, and 280 nm, respectively.

6. Atmospheric pressure solid analysis probe-mass spectrometry (ASAP-MS)

Atmospheric pressure solid analysis probe-mass spectrometry (ASAP-MS) was performed using a Zspray™ from Waters Corporation (Wilmslow, UK). The source conditions were as follows; positive ion mode source cone voltage of 30 V, desolvation gas flow rate of 600 L/h, and probe temperature of 400 °C. Data were obtained and processed using Masslynx 4.1 from Waters Corporation.

7. Ultraviolet absorption spectroscopy

UV spectra of the BTs and DBTs were recorded using a GeneQuant 1300 from GE Healthcare Bio-sciences Corporation (Massachusetts, USA).

8. Column Chromatography and thin-layer chromatography

Analytical thin-layer chromatography (TLC) was performed on TLC silica gel 60 F_{254} plates from Merck (Darmstadt, Germany). Flush column chromatography was performed on silica-gel Silica gel 60 N (spherical, neutral particle size 40–100 μm) from Kanto Chemical Co., Inc. (Tokyo, Japan).

Substrate synthesis

1. Synthesis of 4-methyldibenothiohene (4-MDBT)

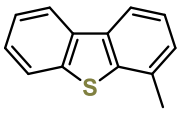

4-MDBT

A 200 mL, two-necked, round-bottomed flask was equipped with a magnetic stirring bar. The flask was dried using a heat gun under a high vacuum and then flushed with nitrogen. THF (3.8 mL) and dibenzothiophene (1.81 g, 9.8 mmol, 1 equiv) were mixed in the flask. The solution was cooled to −78°C, then BuLi (1.6 M in hexane, 19 mL, 29.4 mmol, 3 equiv) was added dropwise via a syringe, and the resultant solution was stirred at room temperature for 5 h. The resulting solution was cooled to −78 °C, and iodomethane (1.9 mL, 29.4 mmol, 3 equiv) was added dropwise via a syringe. After stirring the solution for 12 h at room temperature, the reaction was quenched with cold water. The solution was extracted with $CHCl_3$ (50 mL × 3 times). The $CHCl_3$ extracts were combined, dried over $MgSO_4$, filtrated and evaporated. The crude product was purified by silica-gel column chromatography (hexane, *Rf* = 0.8) and afforded 1.2 g (59%) of 4-MDBT as a white solid.

^{1}H NMR [600 MHz, $(CD_3)_2CO$]: δ 8.30 (m, 1H), 8.16 (d, *J* = 8.4 Hz, 1H), 8.00 (m, 1H), 7.52 (m, 2H), 7.45 (t, *J* = 7.5 Hz, 1H), 7.35 (d, *J* = 8.4 Hz, 1H), 2.57 (s, 3H).

^{13}C{^{1}H}NMR [150 MHz, $(CD_3)_2CO$]: δ140.0, 139.8, 137.0, 136.2, 132.9, 128.0, 127.7, 125.9, 125.5, 123.7, 122.8, 120.2, 20.4.

Experiments

1. Photodecomposition experiments and calculation of the reaction rate constants of BTs and DBTs

Cyclohexane was used as a model solution for the fuel. BT, 2-MBT, DBT, 4-MDBT, or 4,6-DMDBT were dissolved in cyclohexane, respectively. The concentrations were adjusted to 0.54 mmol/L. A 3 mL aliquot of a sample solution was transferred to a two-faced clear quartz cell with a lid, stirred with a magnetic stirrer, and irradiated UV light at room temperature under atmospheric pressure. The amount of degradation of a sample was measured by GC-FID at 0.25, 0.75, 1, 1.5 and 2 h (BT), 1, 2, 3, 4, 5 and 6 h (2-MBT), or 2, 4, 6, 12, 14 and 16 h (DBT, 4-MDBT and 4,6-DMDBT).

For photodegradation experiments of solutions containing high concentrations of sulfur, cyclohexane solutions of BT, 2-MBT, DBT, 4-MDB and 4,6-DMDBT (sulfur content: 20 mg(S)/L (= 0.62 mmol/L), total sulfur content: 100 mg(S)/L (= 3.1 mmol/L) were transferred into 3 mL quartz tubes and irradiated with UV light. The quartz tubes were then irradiated with UV light at room temperature under atmospheric pressure. The amount of decomposition of the solution was measured by GC-FID after 24, 48 and 60 h.

Unless otherwise stated, the solution was irradiated with UV light and left at room temperature and atmospheric pressure. The degradation efficiency (%) of BTs and DBTs were calculated using equation (1).

$$\text{Degradation efficiency (\%)} = \frac{(C_0 - C)}{C_0} \times 100 \qquad (1)$$

C_0 and C were BT or DBT concentrations (mmol/L) before and after UV irradiation, respectively.

2. Photodecomposition reaction of DBT-d_8

A 0.54 mmol/L DBT-d_8 was prepared in *trans*-decalin. A 3 mL aliquot of this solution was transferred to a two-face clear quartz cell, stirred with a magnetic stirrer and irradiated with UV light at room temperature under atmospheric pressure for 24 h. GC-MS analyzed the solution after the removal of yellow precipitates.

3. XRF analysis of precipitates

The yellow precipitates formed after 8W UV irradiation (24 h) of BTs and DBTs were dissolved in acetone, and the whole amounts were impregnated in filter paper (φ21 mm) for XRF analysis. In addition, the relationship between XRF peak intensity and sulfur content was investigated to determine the amount of sulfur precipitated. The standard solutions with sulfur contents of 50, 100 and 200 mg(S)/L were prepared for quantitative analysis, where 25, 50 and 100 μg of sulfur are contained in 0.5 mL of each standard solution.

4. Identification of precipitates using HPLC and ASAP-MS

A sample was prepared and irradiated as described in section 2–3. The same operation was performed 8 times and the precipitates were collected. The collected yellow precipitates were dissolved in acetone, filtered (0.22 μm), and purified by HPLC. A purified sample was dried in a vacuum overnight and analyzed by ASAP-MS.

5. Estimation of molar ratio of O_2, BTs and DBTs

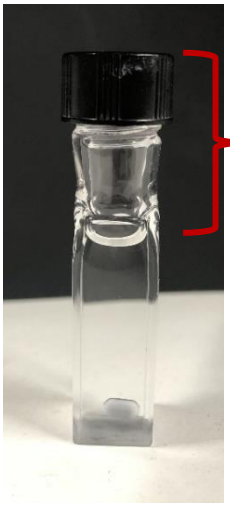

Dead space volume (1.5 mL)

Percentage of oxygen in the air 21%

1.5 mL × 0.21 = 0.32 mL

Amount of mol of oxygen present in dead space

1 mol : 22400 mL (standard state) = x : 0.32 mL

x = 14.3 µmol

Oxygen content in cyclohexane

The solubility of oxygen in cyclohexane was calculated from Pagano et al. (2014) report.

75.5 mg/L × 0.003 L (amount used in the experiment)

= 0.227 mg

0.227 mg / 32 g/mol

= 0.00709 mmol

= 7.09 µmol

Total oxygen amount

14.3 µmol + 7.09 µmol = <u>21.4 µmol</u>

BTs and DBTs amounts

0.54 mmol/L × 0.003 L (amount used in the experiment) = <u>1.62 µmol</u>

The molar ratio of O_2 to BTs and DBTs were estimated to be roughly more than 10 times higher.

Cartesian coordinates for stationary point

1. DBTO

S	-0.000001	1.765442	-0.359182
C	-1.270090	0.480679	-0.126292
C	-0.735949	-0.815145	-0.032419
C	0.735949	-0.815145	-0.032420
C	1.270090	0.480680	-0.126290
C	2.637140	0.724797	-0.105356
C	3.503103	-0.368049	0.019011
C	2.990576	-1.668775	0.096800
C	1.612261	-1.900822	0.069082
C	-2.637141	0.724795	-0.105356
C	-3.503104	-0.368050	0.019009
C	-2.990575	-1.668776	0.096801
C	-1.612260	-1.900823	0.069089
H	3.022748	1.737865	-0.170334
H	4.575970	-0.205319	0.052578
H	3.672082	-2.509721	0.184070
H	1.230533	-2.915457	0.134674
H	-3.022749	1.737863	-0.170341
H	-4.575970	-0.205321	0.052576
H	-3.672080	-2.509722	0.184069
H	-1.230530	-2.915457	0.134679
O	-0.000001	2.763250	0.786874

2. TS1 for (DBTO --> DBSO)

S	1.7796916905	-0.1369531501	-0.0777281647
C	0.5970997600	0.9651528833	0.7782463349
C	-0.7185061199	0.6450405184	0.3832016861
C	-0.7780311500	-0.3971740103	-0.6120303437
C	0.4753633883	-0.9668547369	-0.8915376980

C	0.6270087422	-2.0612913919	-1.7301322277
C	-0.4970179194	-2.5938615630	-2.3282930991
C	-1.7473918707	-2.0225560099	-2.0878322942
C	-1.8965677222	-0.9405611383	-1.2444443612
C	0.8557606469	1.7647973072	1.9009646545
C	-0.2182377206	2.3146836337	2.5507554194
C	-1.5377564806	2.0851697970	2.1307663710
C	-1.7754216174	1.2522818586	1.0632980366
H	1.6037057651	-2.4753262975	-1.9197702527
H	-0.4086003586	-3.4390308505	-2.9894517547
H	-2.6175417316	-2.4387651905	-2.5688012419
H	-2.8746182046	-0.5247396360	-1.0689653845
H	1.8666211267	1.9592639149	2.2107093050
H	-0.0375330244	2.9388635320	3.4110681846
H	-2.3571337357	2.5425167761	2.6574461448
H	-2.7877188101	1.0390351170	0.7588855926
O	1.7268283460	1.3953096366	-0.5953539073

3. DBSO

S	1.3767986642	1.7590768107	0.7394788392
C	-1.0175539220	1.5213531920	-0.1272041500
C	-0.9975570880	0.1300945803	-0.0088310832
C	0.2854004538	-0.5944858703	-0.0713591494
C	1.4771000240	0.0691023559	0.2436972003
C	2.6974908552	-0.5845157473	0.2072852692
C	2.7499103982	-1.9257875590	-0.1337787117
C	1.5855764964	-2.5925835178	-0.4763696142
C	0.3710503759	-1.9278571793	-0.4596745992
C	-2.1987267103	2.2370862319	-0.1331858106
C	-3.4014502493	1.5656230802	0.0015677763
C	-3.4115090689	0.1879609248	0.1538474060

C	-2.2209752394	-0.5161725405	0.1506437563
H	3.6013009877	-0.0440841723	0.4362397230
H	3.6979025847	-2.4370109890	-0.1561829380
H	1.6229161348	-3.6280708999	-0.7715494966
H	-0.5211469335	-2.4504859448	-0.7604149210
H	-2.1548907876	3.3071398478	-0.2412329878
H	-4.3255078520	2.1196070072	0.0033679371
H	-4.3433811050	-0.3370066774	0.2811874727
H	-2.2389535997	-1.5843475236	0.2871886427
O	0.1532045809	2.2183645904	-0.3097205613

4. DBSXO

S	1.4607631117	0.9926181257	1.5981547498
C	-1.0363362847	1.4235512911	-0.6095082681
C	-0.9293885709	0.0207313592	-0.1943190868
C	0.3657591277	-0.6764384847	-0.3044432060
C	1.5130532041	-0.2680689405	0.4143985596
C	2.7154593882	-0.9624203764	0.2243364907
C	2.7888102422	-2.0505581104	-0.6215166053
C	1.6541144855	-2.4632462770	-1.3019819061
C	0.4586326407	-1.7797457017	-1.1429056457
C	-2.3420830793	2.0463332864	-0.4998236954
C	-3.4280256968	1.3492195974	-0.0668325133
C	-3.2976635531	-0.0030830046	0.2868021544
C	-2.0591641568	-0.6460046729	0.2103665069
H	3.5834889344	-0.6335024284	0.7692851608
H	3.7216812982	-2.5738969907	-0.7490369518
H	1.6985586573	-3.3113891377	-1.9654148202
H	-0.4125488455	-2.0909534796	-1.6950823502
H	-2.4013167121	3.0812881733	-0.7905614956
H	-4.3913239283	1.8268149698	0.0045832533

H	-4.1587152961	-0.5519176097	0.6294770481
H	-1.9846747011	-1.6811427542	0.5014557724
O	-0.0760812652	2.0428111656	-1.0644331514

5. DBFES

S	2.0791622387	0.3323872030	1.5501167426
C	-1.0001910553	1.1274465479	-0.2513182946
C	-1.2602782489	-0.2374374433	-0.1133697748
C	0.0325738583	-0.8808848454	-0.0840853437
C	0.9909715857	0.2283702500	0.0574733679
C	2.4087822587	0.0014232670	-0.2582289409
C	2.7697690020	-1.3757463599	-0.6119386021
C	1.8721432900	-2.3664766278	-0.5874842692
C	0.4656090015	-2.1337600438	-0.3378797277
C	-1.9977965072	2.0666942535	-0.3798838644
C	-3.3056084154	1.6015825482	-0.3595064204
C	-3.5930265886	0.2458432884	-0.2229440228
C	-2.5745151062	-0.6846387989	-0.1050108976
H	2.9580168570	0.8069156046	-0.7181711010
H	3.7938895983	-1.5680296360	-0.8849047878
H	2.1832007582	-3.3699270011	-0.8276894206
H	-0.2321934606	-2.9444206614	-0.4637133833
H	-1.7637552291	3.1113521518	-0.4865954548
H	-4.1148304427	2.3074273542	-0.4482753912
H	-4.6193705878	-0.0801918546	-0.2082638814
H	-2.7977151470	-1.7336504499	-0.0011650258
O	0.3321643405	1.4087212535	-0.2711645064

6. TS2 for (DBSXO --> DBFES)

S	-1.319849	-1.628417	1.358330
C	1.270935	-0.675015	-0.590320

C	0.924326	0.530779	0.159703
C	-0.468466	0.660722	0.199892
C	-1.188120	-0.618088	-0.019605
C	-2.445559	-0.555673	-0.758721
C	-3.098669	0.641628	-0.839159
C	-2.512370	1.825376	-0.283936
C	-1.243036	1.845033	0.254566
C	2.658530	-0.989981	-0.747488
C	3.600956	-0.117212	-0.261737
C	3.253202	1.088380	0.423907
C	1.934543	1.411984	0.624822
H	-2.892783	-1.488395	-1.083212
H	-4.092841	0.697721	-1.271796
H	-3.074367	2.754522	-0.337660
H	-0.786942	2.781963	0.559946
H	2.930060	-1.898580	-1.273926
H	4.654824	-0.346287	-0.401559
H	4.042258	1.733374	0.797260
H	1.658910	2.311970	1.168006
O	0.320103	-1.347402	-1.107736

7. DBTO (S1)

S	0.8794756724	1.8140430463	0.3322718319
C	-0.7989845703	1.3320176998	0.0950710193
C	-1.0315002723	-0.1038314153	0.0753316627
C	0.1777336920	-0.7903901072	-0.0142998896
C	1.2903752679	0.1457860086	-0.0593862891
C	2.5783420454	-0.3308012700	-0.2750379636
C	2.7793452157	-1.6826580351	-0.4366877685
C	1.7032278449	-2.6085667205	-0.3671962325
C	0.4259732612	-2.1754487097	-0.1602080066

C	-1.8823297636	2.2021335430	0.0559832612
C	-3.1583194858	1.6890985264	0.0049502245
C	-3.3979592620	0.2880969007	0.0126400971
C	-2.3581199003	-0.5945131990	0.0470780858
H	3.4117305442	0.3514658042	-0.3048625526
H	3.7756786550	-2.0544917085	-0.6085333590
H	1.9065363239	-3.6593328020	-0.4841280480
H	-0.3917768540	-2.8758002460	-0.1185370233
H	-1.7235145843	3.2676110224	0.0760796223
H	-3.9999914989	2.3605634366	-0.0301013934
H	-4.4125563330	-0.0711575636	-0.0134775644
H	-2.5395577995	-1.6566363220	0.0420134616
O	1.1501988016	2.1054361110	1.7814088243

8. MECI

S	1.4567447879	1.3544558794	1.6425979756
C	-1.0619634305	1.5304760982	-0.5815707953
C	-0.9550985579	0.1902713546	0.0054629563
C	0.3344751314	-0.5247241340	-0.0333170230
C	1.4906980112	-0.0429190473	0.6229340358
C	2.6859612643	-0.7659839806	0.5097442568
C	2.7438258213	-1.9475548700	-0.2009394834
C	1.6006965877	-2.4284680509	-0.8196085128
C	0.4117233971	-1.7206962234	-0.7343484480
C	-2.3630452440	2.1706582334	-0.5316903628
C	-3.4451011721	1.5412536312	0.0031063694
C	-3.3151597635	0.2435770506	0.5223841213
C	-2.0813409041	-0.4123367213	0.5080997951
H	3.5606264228	-0.3819580326	1.0056924101
H	3.6712134282	-2.4911620927	-0.2711391292
H	1.6328117625	-3.3499640934	-1.3772216578

H	-0.4667455176	-2.0884631658	-1.2379846661
H	-2.4220210975	3.1608486876	-0.9502230584
H	-4.4049735088	2.0302848939	0.0282892591
H	-4.1729706147	-0.2518018572	0.9450924799
H	-2.0074627546	-1.4035758828	0.9250827970
O	-0.1058950485	2.0807823235	-1.1254433199

9. DBT

S	0.000000	1.971277	-0.000037
C	-1.260056	0.732511	0.000009
C	-0.727835	-0.577870	-0.000020
C	0.727835	-0.577871	-0.000020
C	1.260056	0.732511	0.000009
C	2.639351	0.962240	0.000035
C	3.497719	-0.135967	0.000031
C	2.987040	-1.445291	0.000006
C	1.613132	-1.668238	-0.000019
C	-2.639352	0.962240	0.000034
C	-3.497719	-0.135966	0.000032
C	-2.987040	-1.445291	0.000006
C	-1.613132	-1.668238	-0.000021
H	3.035041	1.973273	0.000043
H	4.571699	0.024736	0.000040
H	3.670121	-2.289269	0.000004
H	1.226284	-2.683266	-0.000029
H	-3.035042	1.973273	0.000038
H	-4.571699	0.024734	0.000043
H	-3.670121	-2.289268	0.000006
H	-1.226283	-2.683266	-0.000036

10. 4-MDBT

S	0.063714	-1.787169	0.000001
C	1.090069	-0.345297	-0.000007
C	0.335552	0.849634	0.000003
C	-1.097560	0.594462	0.000001
C	-1.393101	-0.788119	-0.000002
C	-2.710952	-1.255615	-0.000004
C	-3.748093	-0.324387	-0.000002
C	-3.473607	1.053998	0.000002
C	-2.159770	1.513534	0.000003
C	2.495027	-0.352391	-0.000016
C	3.129571	0.893191	-0.000012
C	2.401466	2.094486	0.000003
C	1.010978	2.080578	0.000007
H	-2.923683	-2.320310	-0.000005
H	-4.777547	-0.670092	-0.000004
H	-4.293624	1.765722	0.000004
H	-1.955970	2.580472	0.000006
C	3.272229	-1.644472	0.000011
H	4.215949	0.927594	-0.000025
H	2.932838	3.041490	0.000002
H	0.452691	3.012091	0.000013
H	3.035322	-2.251694	0.882460
H	4.348994	-1.456107	-0.000379
H	3.034747	-2.252088	-0.882008

11. 4,6-DMDBT

S	-0.000001	1.598665	-0.000002
C	-1.262291	0.359018	-0.000001
C	-0.727834	-0.948719	0.000000

C	0.727835	-0.948718	0.000000
C	1.262291	0.359018	-0.000001
C	2.644351	0.611886	-0.000002
C	3.486891	-0.503557	-0.000002
C	2.979600	-1.813520	0.000000
C	1.608044	-2.042802	0.000001
C	-2.644352	0.611886	-0.000002
C	-3.486892	-0.503556	-0.000001
C	-2.979600	-1.813519	0.000002
C	-1.608045	-2.042802	0.000002
C	3.183989	2.019899	0.000004
H	4.562589	-0.347609	-0.000006
H	3.668287	-2.653141	-0.000001
H	1.221018	-3.057481	0.000003
C	-3.183986	2.019900	0.000001
H	-4.562590	-0.347609	-0.000003
H	-3.668287	-2.653141	0.000003
H	-1.221022	-3.057482	0.000003
H	-2.844388	2.576645	0.882198
H	-4.277131	2.022336	-0.000068
H	-2.844275	2.576694	-0.882120
H	4.277134	2.022330	-0.000063
H	2.844391	2.576643	0.882200
H	2.844282	2.576696	-0.882117

12. DBT-O_2 (σ-complex)

S	-0.000022	-1.493048	-1.049425
C	-1.261672	-0.346979	-0.594268
C	-0.730118	0.850673	-0.066581
C	0.729976	0.850714	-0.066618
C	1.261573	-0.346906	-0.594339

C	2.638203	-0.562930	-0.693582
C	3.498486	0.447493	-0.267093
C	2.988793	1.648760	0.252537
C	1.615008	1.853906	0.354199
C	-2.638292	-0.563083	-0.693446
C	-3.498614	0.447290	-0.266911
C	-2.988966	1.648585	0.252695
C	-1.615186	1.853811	0.354285
H	3.029568	-1.494284	-1.090350
H	4.571973	0.301035	-0.336244
H	3.673459	2.424817	0.580725
H	1.231382	2.784578	0.761418
H	-3.029623	-1.494460	-1.090195
H	-4.572096	0.300770	-0.336011
H	-3.673661	2.424601	0.580919
H	-1.231593	2.784505	0.761483
O	0.000119	-2.402224	1.422316
O	0.000606	-1.451623	2.219405

13. 4-MDBT-O_2 (σ-complex)

S	-0.004321	-1.380072	-0.840566
C	-0.907194	0.085396	-0.472052
C	-0.068537	1.138887	-0.038150
C	1.337194	0.747860	-0.014182
C	1.522581	-0.592103	-0.420418
C	2.787567	-1.179965	-0.471776
C	3.891783	-0.408206	-0.107362
C	3.728476	0.925498	0.297564
C	2.461051	1.504752	0.344530
C	-2.305461	0.203176	-0.538982
C	-2.843646	1.446220	-0.179551

C	-2.031101	2.510364	0.231517
C	-0.646172	2.365284	0.307442
H	4.884497	-0.846798	-0.137117
H	4.597937	1.512326	0.577645
H	2.345876	2.537832	0.658997
C	-3.173651	-0.942035	-0.991976
H	-3.920992	1.580420	-0.220602
H	-2.488174	3.457445	0.502026
H	-0.025673	3.191947	0.639768
O	-0.944589	-2.327426	1.460641
O	-1.625321	-1.453084	2.022167
H	-4.230220	-0.663972	-0.969238
H	-3.037547	-1.815806	-0.345162
H	-2.925974	-1.246431	-2.016446
H	2.911353	-2.212515	-0.782908

14. 4,6-DMDBT-O_2 (σ-complex)

S	-0.059693	-1.262879	-0.697076
C	-1.404306	-0.183664	-0.291094
C	-0.962453	1.123119	0.008627
C	0.488603	1.248237	-0.083071
C	1.106328	0.033360	-0.460488
C	2.499138	-0.110588	-0.574243
C	3.265955	1.035100	-0.323152
C	2.674758	2.254895	0.029711
C	1.290565	2.369854	0.154320
C	-2.756478	-0.556322	-0.264427
C	-3.672820	0.446186	0.074901
C	-3.259766	1.752903	0.373129
C	-1.910755	2.098989	0.342169
C	3.128659	-1.423306	-0.962901

H	4.347369	0.967767	-0.403292
H	3.305100	3.119178	0.216291
H	0.842468	3.316288	0.441132
C	-3.194476	-1.964791	-0.577510
H	-4.730468	0.199054	0.108988
H	-4.002447	2.501512	0.632094
H	-1.598435	3.112427	0.575102
O	0.774364	-2.227706	1.632556
O	1.610861	-1.453180	2.127325
H	2.787713	-1.749088	-1.953441
H	2.865472	-2.210241	-0.247436
H	4.217956	-1.340649	-0.991838
H	-4.281638	-2.059767	-0.518076
H	-2.753356	-2.682281	0.124665
H	-2.884159	-2.264875	-1.585854

15. DBT-O_2 (σ-complex)--DBT (TS)

S	-2.685222	-1.875775	0.552969
C	-3.199977	-0.153421	0.392777
C	-2.672577	0.456731	-0.755542
C	-1.776320	-0.434516	-1.508752
C	-1.648134	-1.698789	-0.913672
C	-0.845236	-2.701596	-1.436430
C	-0.126187	-2.420428	-2.603770
C	-0.243425	-1.169899	-3.220614
C	-1.067596	-0.175590	-2.684273
C	-4.058968	0.496258	1.266717
C	-4.398756	1.824197	0.982672
C	-3.893803	2.451739	-0.161883
C	-3.035947	1.776257	-1.035934
H	-0.756544	-3.664249	-0.943185

H	0.528339	-3.175451	-3.027255
H	0.317927	-0.965065	-4.127143
H	-1.141748	0.791388	-3.172153
H	-4.438399	-0.001046	2.153698
H	-5.056725	2.366808	1.654048
H	-4.170314	3.479958	-0.375157
H	-2.649614	2.279596	-1.916832
O	-1.778959	-2.036452	1.818815
O	-0.594721	-0.837187	1.756091
S	1.184168	0.457381	1.890775
C	2.392939	-0.602715	1.161974
C	3.130030	0.023041	0.131247
C	2.694033	1.395500	-0.091739
C	1.644517	1.761209	0.784625
C	1.073649	3.037336	0.742247
C	1.558740	3.958608	-0.185762
C	2.602566	3.611354	-1.060442
C	3.169613	2.339158	-1.015247
C	2.623051	-1.932092	1.524721
C	3.622619	-2.638834	0.857409
C	4.376206	-2.029182	-0.161060
C	4.131821	-0.707697	-0.527399
H	0.268375	3.304641	1.420016
H	1.127463	4.954729	-0.228649
H	2.973056	4.341668	-1.773896
H	3.980167	2.080530	-1.691124
H	2.020783	-2.398295	2.297134
H	3.818804	-3.672567	1.127596
H	5.153652	-2.593804	-0.667608
H	4.713955	-0.245207	-1.319854

16. 4-MDBT-O_2 (σ-complex)--4-MDBT (TS)

S	1.737918	-1.985259	2.544889
C	1.312864	-0.345311	3.166817
C	-0.027570	-0.017969	2.908215
C	-0.720643	-1.043247	2.112506
C	0.107082	-2.129085	1.791522
C	-0.321585	-3.208618	1.032949
C	-1.638643	-3.192055	0.560689
C	-2.487216	-2.124174	0.874560
C	-2.039713	-1.051452	1.651550
C	2.192983	0.479165	3.868931
C	1.657420	1.691432	4.335510
C	0.320838	2.035287	4.110341
C	-0.532265	1.188041	3.398592
H	-1.999670	-4.009510	-0.055120
H	-3.508042	-2.125034	0.504654
H	-2.709693	-0.228454	1.880366
C	3.642273	0.118331	4.073220
H	2.302943	2.374725	4.880266
H	-0.058093	2.978856	4.491801
H	-1.565363	1.470421	3.222660
O	2.832971	-1.869909	1.431633
O	2.368840	-0.655294	0.352080
S	1.970496	0.684196	-1.355273
C	1.148936	-0.437917	-2.441475
C	-0.087670	0.055782	-2.913533
C	-0.392241	1.372697	-2.368580
C	0.630113	1.834832	-1.507933
C	0.562539	3.081696	-0.862616
C	-0.574002	3.859356	-1.107453

C	-1.599964	3.420045	-1.960454
C	-1.515173	2.183078	-2.593629
C	1.627497	-1.696313	-2.814100
C	0.862823	-2.464221	-3.691453
C	-0.363994	-1.984628	-4.182938
C	-0.841561	-0.734615	-3.795792
C	1.671321	3.551365	0.045313
H	-0.659300	4.830310	-0.625626
H	-2.464694	4.055530	-2.128774
H	-2.308697	1.850706	-3.256937
H	1.219764	-3.443908	-3.996353
H	-0.944955	-2.594538	-4.868800
H	-1.793479	-0.373311	-4.175272
H	1.434806	4.524967	0.483647
H	2.617110	3.646967	-0.502483
H	1.845407	2.838339	0.859454
H	4.136886	0.845368	4.721917
H	4.167006	0.090465	3.112448
H	3.750673	-0.872067	4.530911
H	2.565392	-2.064124	-2.411806
H	0.349326	-4.026947	0.791958

17. 4,6-DMDBT-O_2 (σ-complex)--4,6-DMDBT (TS)

S	2.266410	-2.060109	-0.239859
C	3.019653	-0.431683	-0.071319
C	2.576601	0.228085	1.085232
C	1.533491	-0.519770	1.804252
C	1.207443	-1.734675	1.182115
C	0.227498	-2.610526	1.651429
C	-0.443149	-2.210169	2.818703
C	-0.130190	-1.012323	3.468159

C	0.858699	-0.159524	2.972201
C	3.981022	0.084209	-0.942328
C	4.511930	1.337807	-0.595824
C	4.102990	2.010709	0.560135
C	3.136937	1.465758	1.409406
C	-0.129053	-3.882977	0.926827
H	-1.228378	-2.846830	3.216299
H	-0.670366	-0.738286	4.369435
H	1.085864	0.772182	3.480241
C	4.395250	-0.635522	-2.200755
H	5.255790	1.790281	-1.245675
H	4.541922	2.975194	0.798081
H	2.822198	2.001656	2.299096
O	1.412621	-2.132671	-1.551944
O	0.332433	-0.830257	-1.596547
S	-1.280620	0.700933	-1.815090
C	-2.663808	-0.089641	-1.048414
C	-3.149089	0.626035	0.068154
C	-2.388218	1.845423	0.309144
C	-1.349880	2.015421	-0.634333
C	-0.482590	3.120923	-0.610694
C	-0.690817	4.063839	0.401077
C	-1.717843	3.916300	1.348241
C	-2.567916	2.814540	1.307789
C	-3.229612	-1.302916	-1.475080
C	-4.317470	-1.779662	-0.735854
C	-4.821293	-1.083039	0.375212
C	-4.244910	0.116658	0.781869
C	0.611301	3.275361	-1.636764
H	-0.041256	4.934513	0.448468
H	-1.850824	4.673879	2.115371

H	-3.364263	2.708657	2.038981
C	-2.684156	-2.040608	-2.671312
H	-4.783343	-2.715309	-1.035317
H	-5.670579	-1.486558	0.919303
H	-4.638477	0.652158	1.641170
H	-1.597400	-2.154188	-2.587510
H	-2.879173	-1.483528	-3.597126
H	-3.147916	-3.026349	-2.770194
H	1.212414	4.167356	-1.439677
H	0.194386	3.364166	-2.647848
H	1.274484	2.402837	-1.640131
H	0.756533	-4.500386	0.735178
H	-0.581644	-3.654278	-0.043412
H	-0.836199	-4.477545	1.510200
H	5.215302	-0.110740	-2.696933
H	3.553002	-0.708429	-2.896595
H	4.727908	-1.658406	-1.987896

18. DBTDX

S	0.000406	-1.470877	-1.155209
C	-1.156550	-0.627437	0.087049
C	-0.687148	0.815754	0.064056
C	0.687185	0.815671	0.064174
C	1.156478	-0.627166	0.087406
C	2.610063	-0.852537	-0.075189
C	3.440974	0.211451	-0.175083
C	2.969202	1.581772	-0.102061
C	1.641295	1.874923	0.025755
C	-2.609966	-0.852558	-0.075788
C	-3.441086	0.211216	-0.175250
C	-2.969378	1.581741	-0.101853

C	-1.641472	1.874775	0.025951
H	2.968868	-1.875817	-0.090224
H	4.507181	0.043660	-0.300117
H	3.699983	2.382840	-0.151745
H	1.303587	2.906199	0.071125
H	-2.968715	-1.875876	-0.091142
H	-4.507296	0.043570	-0.300365
H	-3.700249	2.382736	-0.151112
H	-1.303844	2.906101	0.071570
O	0.734053	-1.213987	1.345739
O	-0.734504	-1.214140	1.345555

19. DBTDX dimer

S	-1.470009	1.518014	1.987383
C	-0.704630	1.541356	3.715053
C	-0.154575	2.949864	3.834292
C	0.450420	3.272238	2.643304
C	0.316364	2.084261	1.708219
C	0.763871	2.281127	0.310697
C	1.312880	3.466166	-0.044810
C	1.508722	4.554162	0.895669
C	1.104587	4.458490	2.196588
C	-1.539896	1.061210	4.838420
C	-1.720394	1.854732	5.920341
C	-1.103742	3.162566	6.043235
C	-0.338378	3.687463	5.041082
H	0.660539	1.456509	-0.386529
H	1.638421	3.610482	-1.071173
H	1.990428	5.460943	0.543000
H	1.252042	5.284607	2.886130
H	-1.973207	0.069665	4.765321

H	-2.339771	1.502331	6.740661
H	-1.263918	3.725532	6.957360
H	0.109729	4.671567	5.143702
O	1.072131	0.979632	2.284575
O	0.426387	0.636212	3.559177
S	-1.470009	-1.210838	-1.358381
C	-0.704630	-1.234180	-3.086051
C	-0.154575	-2.642688	-3.205290
C	0.450420	-2.965062	-2.014302
C	0.316364	-1.777085	-1.079217
C	0.763871	-1.973951	0.318305
C	1.312880	-3.158990	0.673812
C	1.508722	-4.246986	-0.266667
C	1.104587	-4.151314	-1.567586
C	-1.539896	-0.754034	-4.209418
C	-1.720394	-1.547556	-5.291339
C	-1.103742	-2.855390	-5.414233
C	-0.338378	-3.380287	-4.412080
H	0.660539	-1.149333	1.015531
H	1.638421	-3.303306	1.700175
H	1.990428	-5.153767	0.086002
H	1.252042	-4.977431	-2.257128
H	-1.973207	0.237511	-4.136319
H	-2.339771	-1.195155	-6.111659
H	-1.263918	-3.418356	-6.328358
H	0.109729	-4.364391	-4.514700
O	1.072131	-0.672456	-1.655573
O	0.426387	-0.329036	-2.930175

20. DBTDX (TS for DBT-O_2 (π-complex) --> DBTDX)

S	-0.000000	-1.713566	-0.915220

C	-1.196845	-0.616790	-0.138629
C	-0.699277	0.762220	-0.188885
C	0.699278	0.762220	-0.188885
C	1.196845	-0.616790	-0.138629
C	2.621038	-0.844327	-0.187761
C	3.460370	0.229861	-0.122715
C	2.966184	1.578768	-0.062264
C	1.620441	1.840454	-0.091243
C	-2.621038	-0.844327	-0.187761
C	-3.460370	0.229861	-0.122715
C	-2.966184	1.578768	-0.062264
C	-1.620441	1.840454	-0.091243
H	2.998210	-1.860357	-0.228124
H	4.534851	0.069694	-0.122262
H	3.678088	2.395447	0.003545
H	1.254525	2.862181	-0.059488
H	-2.998210	-1.860357	-0.228124
H	-4.534850	0.069694	-0.122263
H	-3.678088	2.395447	0.003545
H	-1.254525	2.862181	-0.059489
O	0.680127	-0.932445	1.559634
O	-0.680127	-0.932445	1.559634

21. DBT-O_2 (π-complex)

S	0.000008	-1.952706	-0.478226
C	-1.257870	-0.714814	-0.430829
C	-0.724838	0.598208	-0.389513
C	0.724681	0.598289	-0.389692
C	1.257794	-0.714666	-0.430786
C	2.637946	-0.942254	-0.449985
C	3.492736	0.156418	-0.422875

C	2.982353	1.467340	-0.375509
C	1.611351	1.690525	-0.357516
C	-2.638005	-0.942487	-0.450015
C	-3.492875	0.156106	-0.422656
C	-2.982590	1.467077	-0.375039
C	-1.611621	1.690371	-0.357088
H	3.034686	-1.952074	-0.482404
H	4.566870	-0.002543	-0.435695
H	3.666727	2.309646	-0.350430
H	1.223339	2.704018	-0.318630
H	-3.034659	-1.952329	-0.482629
H	-4.566997	-0.002927	-0.435462
H	-3.667039	2.309316	-0.349740
H	-1.223688	2.703888	-0.318035
O	0.614195	-0.122343	2.496132
O	-0.613412	-0.119455	2.495576

22. DBT (T1)

S	-0.0000016035	1.9896217963	-0.0000000000
C	1.2703080985	0.7430365333	0.0000000000
C	0.6889933070	-0.5993095222	-0.0000000000
C	-0.6889898850	-0.5993126419	0.0000000000
C	-1.2703079524	0.7430317631	-0.0000000000
C	-2.6210047777	0.9458976571	-0.0000000000
C	-3.4913037956	-0.1909345498	-0.0000000000
C	-2.9646307132	-1.5022447086	-0.0000000000
C	-1.6086899491	-1.7324952584	-0.0000000000
C	2.6210044340	0.9458984324	-0.0000000000
C	3.4913032859	-0.1909347124	-0.0000000000
C	2.9646304841	-1.5022445110	-0.0000000000
C	1.6086895805	-1.7324944928	0.0000000000

H	-3.0404038830	1.9477308174	0.0000000000
H	-4.5653332017	-0.0371743482	-0.0000000000
H	-3.6511466438	-2.3450841678	0.0000000000
H	-1.2106903252	-2.7417306170	-0.0000000000
H	3.0404072521	1.9477298911	-0.0000000000
H	4.5653325971	-0.0371747418	0.0000000000
H	3.6511464793	-2.3450834973	-0.0000000000
H	1.2106872117	-2.7417291218	-0.0000000000

23. 4-MDBT (T1)

S	0.0010353728	1.9800646813	-0.0042815702
C	1.2726835749	0.7284391483	-0.0023593065
C	0.6887959169	-0.6088997205	-0.0031315084
C	-0.6896380444	-0.6076164803	-0.0040117881
C	-1.2689361270	0.7372399760	-0.0021064962
C	-2.6204724897	0.9431442276	0.0027695211
C	-3.4916944590	-0.1889558007	0.0049480216
C	-2.9665369424	-1.5033577379	0.0005935505
C	-1.6125371009	-1.7375437733	-0.0043949135
C	2.6235538952	0.9544915523	-0.0002103198
C	3.4813294115	-0.2027760003	0.0014715960
C	2.9587224484	-1.5132361043	0.0012298514
C	1.6032549909	-1.7457944023	-0.0011514594
H	-3.0368576390	1.9462326373	0.0053856665
H	-4.5655576374	-0.0339664102	0.0097909493
H	-3.6554414458	-2.3443052336	0.0013273645
H	-1.2180894094	-2.7482442983	-0.0088250541
C	3.2070476013	2.3444092495	-0.0005337252
H	4.5562542021	-0.0500506589	0.0035604219
H	3.6489208018	-2.3529727206	0.0032485312
H	1.2045282768	-2.7546235933	-0.0012767258

H	4.3002384395	2.3161176606	0.0170611140
H	2.8736401128	2.9196928217	0.8727775023
H	2.9017562501	2.9075109799	-0.8918812228

24. 4,6-DMDBT (T1)

S	-0.0001019987	1.9715167367	0.0075624867
C	1.2712422412	0.7234639569	0.0074413554
C	0.6893211578	-0.6164198215	0.0010108103
C	-0.6892584470	-0.6164741935	0.0008694893
C	-1.2712452805	0.7234350302	0.0074186942
C	-2.6231280579	0.9517104347	0.0079912837
C	-3.4810483311	-0.2012128793	0.0006595079
C	-2.9596732194	-1.5147518977	-0.0059484336
C	-1.6061872133	-1.7506986571	-0.0054453165
C	2.6230890092	0.9516798957	0.0075729661
C	3.4811164471	-0.2013131636	0.0005466680
C	2.9596984358	-1.5147774431	-0.0052057401
C	1.6061713892	-1.7507409238	-0.0045666292
C	-3.2029946112	2.3436028010	0.0049416326
H	-4.5559095013	-0.0478204774	0.0008186526
H	-3.6521894079	-2.3527196093	-0.0110865875
H	-1.2100916618	-2.7605798527	-0.0102273053
C	3.2030770209	2.3434691313	0.0027749185
H	4.5559714065	-0.0478047181	0.0006843290
H	3.6521874185	-2.3527504330	-0.0093482008
H	1.2100576808	-2.7606421913	-0.0085259989
H	4.2929345863	2.3195932563	0.0931055664
H	2.8109700232	2.9451213998	0.8325033823
H	2.9560358957	2.8763040529	-0.9248131296
H	-2.8178736789	2.9411793223	0.8409489954
H	-4.2935651211	2.3191714338	0.0867493245

H	-2.9486061811	2.8804588094	-0.9184327213

Conference presentation

1. Development of an efficient desulfurization method for aromatic organic sulfur compounds in fuel using ultraviolet light

   Taka-Aki SHINOZAKI., Masahiko SUENAGA., Yohan KO., Eiji YAMAMOTO., Haruno MURAYAMA., Makoto TOKUNAGA

   The 12th International Conference on Environmental Catalysis (ICEC-2022), July 30-August

2. 燃料中に含まれるジベンゾチオフェン誘導体の紫外線を用いた効率的な脱硫法の開発

   篠﨑 貴旭・末永 正彦・高 ヨハン・山本 英治・村山 美乃・徳永 信

   第 32 回万有福岡シンポジウム, 2022.06.04.

3. 紫外線を用いた液体燃料に含まれる芳香族硫黄化合物の脱硫法の開発

   篠﨑 貴旭・村山 美乃・徳永 信

   第 11 回 CSJ 化学フェスタ 2021, 2021.10.20.

Award

1. 第 11 回 CSJ 化学フェスタ 2021 (優秀ポスター発表賞), 2021.12.01
2. 第 30 回万有福岡シンポジウム (ベストディスカッション賞), 2020.10.24

Acknowledgment

I would like to express my sincere appreciation to Professor Makoto Tokunaga. He gave me great insight into chemistry and invaluable suggestion, and always warmly encouraged me.

I would like to thank Associate Professor Haruno Murayama for her enthusiastic guidance on a daily basis in conducting this research. She always gave me deep perspective and kind support. I would like to express our sincere appreciation to Lecturer Masahiko Suenaga. He supported my research and gave me insightful advice and discussion.

I would like to thank Assistant Professor Eiji Yamamoto. He gave me precise advice on the experimental results.

I would like to thank Ms. Yukari Uchida, a secretary of the laboratory. She always helped me to handle various procedures and gave kind encouragement.

I am also deeply grateful to Mr. Norio Inami (Toyota Motor Corporation). He gave me a lot of advice from a mechanical engineering perspective.

I would like to thank my laboratory member for making my research life meaningful.

Finally, special thanks are given to my family for their warm encouragement and constant support.

Topics

1. OPTRONICS ONLINE 2022 年 8 月 29 日
2. AdvTech 2022 年 8 月 30 日
3. Yahoo!Japan ニュース 2022 年 9 月 1 日
4. 乗り物ニュース　2022 年 9 月 1 日
5. @nifty ニュース 2022 年 9 月 1 日
6. まいにちニュース 2022 年 9 月 1 日
7. MIT Technology Review Japan 2022 年 9 月 2 日
8. 日刊工業新聞 2022 年 9 月 7 日
9. 日経×Tech 2022 年 9 月 30 日

Patent

1. 含硫化合物を含有している液体燃料の脱硫方法

   特願 2021-87812 2021 年 5 月 25 日

   特開 2022-181001 2022 年 12 月 7 日

List of publications

1. Ultraviolet light-induced decomposition of benzothiophene and dibenzothiophene derivatives for efficient sulfur removal without additives and catalysts.

   T.-A. Shinozaki., M. Suenaga., Y. Ko., E. Yamamoto., H. Murayama., M. Tokunaga.

   J. Clean. Prod., **2022***, 370,* 133402.

2. Study for practical application of supported gold nanoparticles for removal of DMTS responsible for hineka in sake.

   A. Isogai., H. Murayama., M. Kimura., **T. Shinozaki**., E. Yamamoto., T. Fujii., S. Iizuka., M. Tokunaga.

   J. Brew. Soc. Japan., **2019**, *114*, 779-786 (in Japanese).